HUMMAIRA SADAF

The molecular mechanism of PD-L1 overexpression in classical Hodgkin lymphoma (cHL)

Supervisor: Dr hab. n. med. Elżbieta Sarnowska prof. NIO

Co supervisor: Dr n. med. Ryszard Konopinski

The work was performed at the Department of Experimental Immunotherapy of Maria Sklodowska-Curie National Research Institute of Oncology, Warsaw.

Warsaw, 2024

DEDICATION

"This thesis is dedicated to the pursuit of knowledge and the exploration of understanding. May its insights contribute to the betterment and enlightenment of humanity."

ACKNOWLEDGEMENT

"No one who achieves success does so without acknowledging the help of others. The wise and confident acknowledge this help with gratitude".

(Alfred North Whitehead)

My heartfelt gratitude goes to the Director of institute **Prof. Dr hab. n. med. Jan Walewski** and **Prof. Michał Mikula** Deputy Director for Scientific Affairs and head of the Multiscale Research Laboratory of the Genetics Department, Maria Sklodowska-Curie National Research Institute of Oncology for providing me opportunity to enhance my scientific skills in a much better way and fundings to carry out current project.

I wish to express my special thanks to my Supervisor **Prof. Dr. Elzbieta Sarnowska**, Head of the Department of Experimental Immunotherapy and to my Co Supervisor **Dr. Ryszard Konopinski**. I must say without their help, I would not have been able to achieve this milestone.

In last I would like to say my deepest thanks to **all lab members** of the Department Experimental Immunotherapy who really support me in my experiments and **Dear Agnieszka Niewiadomska** Senior administrative specialist for administrative help.

Contents

ABSTRACT

Classical Hodgkin lymphoma is a type of malignancy that originates from abnormal B lymphocytes. It is characterized by bi and multi-nucleated Hodgkin and Reed-Sternberg (HRS) cells. An important hallmark of HRS cells is overexpression of CD30 and PD-L1 (Programmed cell death protein 1 ligand) on the cell surface. Overexpression of PD-L1 plays an important role in proliferation and metabolism of tumor cells. The modern immunotherapy using anti-PD-1/PDL1 antibodies enhances the response of T cell to cancer cells and ultimately blocks the proliferation of HRS cells. For our study we used the three certified HRS cell lines: KM-H2, L-1236, and L428. After 3-5 days, cells from all harvested lines subjected for Western blot analysis with antibodies: anti PD-L1, EZH2 and SWI/SNF subunits to verify in which line the PD-L1 was overexpressed. The immunoprecipitation was performed on L-1236 HRS cells followed by mass spectrometry analysis. The data obtained from this analysis were further confirmed by other methods like Yeast two hybrid system. Furthermore, we performed chromatin immunoprecipitation (ChIP) on L-1236 cHL line using antibodies: anti SWI/SNF (BAF 155), PRC2 complex (EZH2), PD-L1 as well as methylated and acetylated Histone H3 on CD274 promoter region. Furthermore, the MTT assay was performed after the treatment of cells from L1236 cell line with EZH2 inhibitor (EPZ-6438).

We investigated the PD-L1 translocation into cell nuclei and identified its potential nuclear partners in L-1236 cell line. After the mass spectrometry analysis, we found that, PD-L1 may interact in the nucleus with the splicing machinery and thus regulate the RNA posttranscriptional alternative processing. Noteworthy, we subsequently found that the subunits of SWI/SNF (BAF 155), PRC2 complex (EZH2), PD-L1 and methylated and acetylated H3 are located at the same position i.e. (-606) on the promoter region of *CD274* gene that encodes PD-L1 protein. We also analyzed and confirmed the PD-L1 interaction with BAFF155, FUS, SNAIL, and SLUG after Yeast two hybrid assay, all these findings together provide a clue about their involvement in regulating PD-L1 expression and PD-L1 itself in a positive feedback loop manner as well as PDL1 function in the nucleus. The observations after EZH2 inhibitor in HRS cells revealed that EZH2 is not an essential component to be targeted for therapeutic purposes although they are present at PD-L1 loci but there are some additional mechanisms and factors involved in regulation of PD-L1 overexpression that needs further exploration.

1. INTRODUCTION

Hodgkin lymphoma (HL) stands out as the more prevalent lymphoma in the Western world, including Europe and the US, with an annual occurrence of approximately three new cases/100,000 individuals. This lymphoma is categorized into nodular lymphocyte-predominant Hodgkin lymphoma (NLPHL), and classical Hodgkin lymphoma (cHL) (Meti, Esfahani & Johnson, 2018). Multiple genetic mutations, structural variants and multiple mechanisms which include DNA repair, cell cycle, immune evasion, NFκB pathway, and JAK-STAT pathway are associated with Hodgkin lymphoma. These genetic lesions are summarized in the following flow chart (Figure 1.1) (based on Li, Mu and Xiao, 2023).

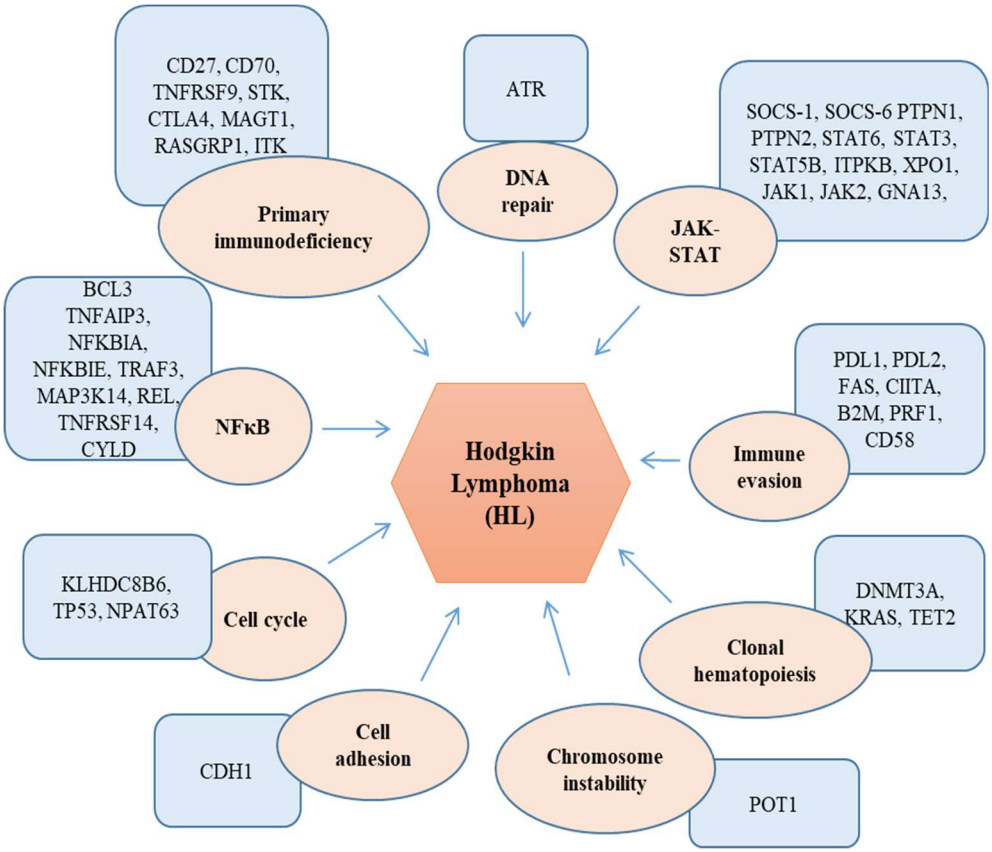

Figure 1.1: Overview of some genetic aberrations in Hodgkin lymphoma. The landscape of different genetic mutations and their respective pathways involved in Hodgkin lymphoma. The mutations in genes e.g., PD-L1, PD-L2 are represented by blue color-coded rectangular blocks while the mechanisms to which they are associated and affected by red color-oval blocks collectively.

1.1: Classical Hodgkin lymphoma (cHL)

The classical Hodgkin Lymphoma (cHL) is characterized as B-cell malignancy, comprising around 10% of all types of lymphomas showing distinctive biological traits, progression patterns, and responses to treatment (Calabretta & Carlo-Stella, 2020). The nomenclature for classical Hodgkin lymphoma (cHL) is linked to the significant contributions of three persons. Thomas Hodgkin in 1832 identified lymphoid lesions and coined the name Hodgkin disease (HD). Afterwards Dorothy Reed and Carl Sternberg in 1902 and 1898 recognized different cell types within HD tissues. The tumor cells in cHL are known as Hodgkin cells (mononucleated) and ReedSternberg cells (multinucleated) as well as Hodgkin and Reed-Sternberg cells (Küppersna & Hansmann, 2005).

There are various distinctive features associated with this type of lymphoma in addition to mononuclear and multinucleated HRS cells, like exhibiting unusual B cell immuno-phenotype, and elevated level of expression of the programmed death-1 ligand PD-L1 (CD274/B7-H1) as well as showing CD30 expression. These specific hallmarks collectively contribute to its uniqueness and differential diagnostic criteria (Aldinucci et al., 2010). It forms four classes: mixed cellularity (MCHL), lymphocyte-depleted (LDHL), lymphocyte-rich (LRHL), and nodular sclerosis (NSHL), (Leeset al., 2019).

Another remarkably interesting fact is that HRS cells constitute just less than 1% of the overall tumor mass (Pileri et al., 2002). The microenvironment of cHL consists of diverse types of inflammatory cells, including immune cells like B and T cells, mast cells, tumor-associated macrophages (TAMs), eosinophils, NK cells and plasma cells. These cells play a significant role in releasing cytokines and chemokines, which are critical for growth, development, and tumor metastasis. There are cascades of signaling mechanisms that occur within the tumor microenvironment, through which these cells interact with the adjacent non-malignant ones and form a complex network. This interplay significantly influences the behavior, progression, and pathogenesis of the disease (Ribatti et al., 2022). The survival rate, expressed as overall survival (OS), is 87% and depends on the factors like disease stage, age of patients and other risks. Despite the optimistic OS, a considerable number of patients still experience the challenge of developing refractory or relapsed classical Hodgkin lymphoma (Smith & Friedman 2022).

1.2: Clinical presentation/features of classical Hodgkin lymphoma

The majority of individuals diagnosed with classical Hodgkin lymphoma (CHL) typically exhibit lymphadenopathy (painless swelling of lymph nodes) as a primary symptom. This condition commonly affects lymph nodes in areas such as the neck (cervical), the chest (mediastinal), above the collarbone (supraclavicular), and in the armpits (axillary), while there may be some variation in the preference for specific sites among different cHL subtypes. Other affected sites beyond the lymph nodes often involve the lungs, liver, and bones (Wang et al., 2019).

Moreover, over 50% of patients develop a chest mass, which can either be asymptomatic or cause breathing difficulties, coughing, or obstruction of the superior vena cava. Around 25% of patients may also experience systemic symptoms like a fever above 38°C, significant weight loss within 6 months, exceeding 10% of their body weight, and night sweats. These symptoms collectively referred to as B symptoms, have important implications for the disease's prognosis (Townsend & Linch, 2012, Jose et al., 2005, Mauch et al., 1993).

1.3: Diagnosis and staging

A proper diagnosis of classical Hodgkin lymphoma requires a thorough tissue biopsy, as techniques like fine needle aspiration may not provide the necessary architectural information. cHL shares similarities with NLPHL in terms of having few cancerous cells and a significant inflammatory backdrop. Although the characteristics of Hodgkin and Reed-Sternberg cells are alike in different subtypes, differences emerge in the surrounding microenvironment (Wang et al., 2019). There are various immune-phenotypic markers also used for classical Hodgkin lymphoma diagnosis as well as its differentiation from other types of lymphomas as described in (Table1.1).

Table 1.1: Immune-phenotypic markers for diagnosis and differentiation of classical Hodgkin lymphoma.

Markers	**+ve/-ve**
CD30, CD15	+ve, membrane and/or Golgi pattern
(PD-L1 /*CD274*, PD-L2/CD273)	+ve

PAX5	+ve but weak
CD45, OCT-2, BCL6, ALK	-ve
IRF4/MUM1	+ve
CD20, CD79a	-ve or weak
T-cell markers	-ve (few cases +ve)
Cytotoxic markers	+ve but in a few cases

There are different immune-phenotypic markers some are positively expressed and present in cHL while others are absent or expressed weakly (as reported by Wang et al., 2019). The (+ve) symbolizes the presence of that particular marker and (–ve) stands for the absence and no expression of that marker.

Hodgkin's lymphoma diagnosis also requires histological analysis. Staging commonly involves contrast-enhanced CT scans of the chest, neck, pelvis, and abdomen. Additionally, functional imaging utilizing 18-F-fluorodeoxyglucose (18-F-FDG) PET (positron emission tomography) is used frequently. It helps in precise disease staging, outlining radiotherapy boundaries, and establishing a starting point for future treatment response evaluation.

There are four stages linked to Hodgkin diseases depending upon the location and the number of involvements of lymph nodes along with some additional symptoms (Harris, 2022). If the mentioned modifying features are present thus denoted by (b) and if absent then mentioned by (a) (based on Townsend & Linch, 2012) as mentioned in (Table 1.2**)**

Table 1.2: Ann Arbor staging system and Cotswolds' modification for classical Hodgkin's Lymphoma.

Stages	**Description**	**Modifying features a" or "b**
Stage I	Participation of only one lymph node area or an extra nodal location.	absence (a) or presence of all or anyone symptoms (b) like unexplained fever, night sweats, and unexplained weight loss
Stage II	The participation of ≥ 2 lymph node regions on the same side of the diaphragm.	

Stage III	The condition where lymph node regions are affected on either side of the diaphragm.	
Stage IV	Participation of extra nodal areas aside from a single, adjoining or nearby extra nodal site.	

1.4: Etiology of classical Hodgkin Lymphoma

The exact cause of Hodgkin Lymphoma remains complex and elusive. Thus far, it has been notably linked to distinct factors such as Epstein Barr Virus (EBV) infection, disruptions in the immune system, and genetic alterations. The risk of developing Hodgkin lymphoma can also be increased by immune suppression, as seen in cases of organ transplants or HIV infection. Additionally, there is a clear familial connection, with a tenfold increase in risk for same-sex siblings, suggesting an interaction between genetics and environmental factors. This complex interplay of viral influences, immune responses, genetic susceptibilities, and ecological elements contributes to the onset of the disease (Kaseb & Babiker, 2023).

1.5: Epidemiology of classical Hodgkin lymphoma

In the United States and European Union, Hodgkin's disease exhibits with occurrence rate of 0.5 cases/100,000 children. It constitutes 5 to 6% of all childhood cancer instances and is positioned as the sixth most frequently diagnosed childhood cancer. It falls in rank behind leukemia, brain tumors, neuroblastomas, and rhabdomyosarcomas in terms of prevalence. The highest incidence of childhood HD is observed in Latin American nations, where it affects approximately 1 to 1.5 children per 100,000. In developing countries, lymphomas, including Hodgkin's disease, are prevalent, with Hodgkin's disease ranking as the fourth most common malignancy, following leukemia, brain tumors, and non-Hodgkin's lymphomas (NHL) (Dinand&Arya, 2006).

CHL shows distinct epidemiological characteristics, notably a bimodal age distribution with geographical and ethnic variations. In developed countries, the initial peak typically occurs towards the end of the 20year of age, followed by a second peak after the age of 50. In contrast, less

developed countries tend to experience the first peak before youth (Medeiros & Greiner, 1995, Grufferman & Delzell, 1984). Furthermore, the male-to-female ratio of Hodgkin Lymphoma shows significantly higher risk in men in comparison to women. The mortality rate was reported to be 1.26 times higher in men than women. It suggests that men may have a worse survival prognosis for HD (Radkiewicz et al., 2023).

In order to study the Hodgkin lymphoma ratio in adults from various parts of the globe, IARC collaborated with GLOBOCAN 2018. The obtained data also showed that it is more prevalent among men. The chance of getting Hodgkin lymphoma in men is 0.10% while in women it is 0.07% (Bray et al., 2018). The death rate in men is recoded approximately 70% more as compared to that of women. Another factor that is associated to the death is lifestyle and income (Huang et al., 2022, Bray et al., 2018). In 2020, almost 83,087 new cases of Hodgkin Lymphoma were reported globally. The occurrence rate was 0.98 per 100,000. It has been noted that incidence rates varied drastically by location. Incidence rates in high-income countries like Europe, Australia and New Zeal and were significantly greater (ASR = 2.6) than those in low-income countries in Asia and Central Africa, ranging from 0.69 to 0.83. Another interesting fact was the variation in the rate of mortality by region. Low-income countries experienced greater mortality rates than highincome ones (Huang et al., 2022).

1.6: Origin and development of HRS cell

The findings revealing mutations in immunoglobulin light and heavy chain V (IgV) genes indicated that HRS cells evolve from mature B-cells either on the stage of GC or post-GC differentiation. The expression of genes, especially B-cell specific, including Syk, BCR, A-myb, CD-19, and CD-20, provides HRS cells with a peculiar and unusual immune phenotype that is a distinctive quality of these cells (Küppers, 2002). Thus, understanding of the mechanism of reprogramming of HRS cell and its potential role in pathogenesis is particularly important. Therefore, many transcription factors that take part in the regulation of B-cell specific genes expression have been studied and it has been found that they are either absent or reduced in HRS cells. Examples of these factors are Bob1, Oct-2, Pu.1, and the early B cell factor (Küppers, 2009).

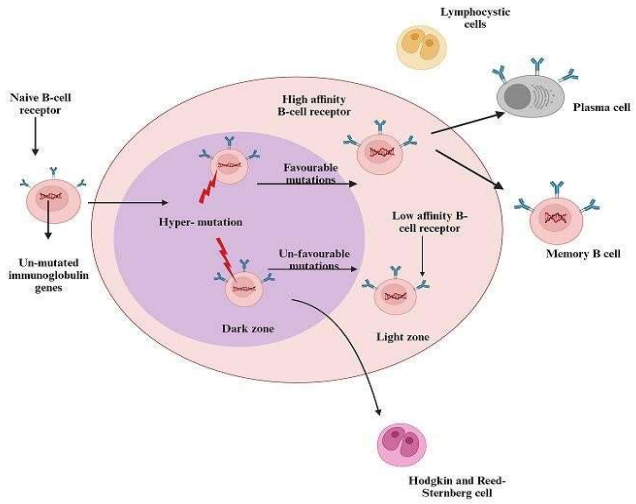

Figure 1.2: Diagrammatic description of the B-cell development and HRS cell production (modified by Bio render from Thomas, Wolf & Diehl, 2004). During the development of B-cell the unfavorable mutation leads to the production of HRS cells rather than production of normal memory B-cell and plasma cell in germinal center (GC) of lymph tissue.

1.7: Immunotherapy

Cancer is a major global health problem with significant morbidity and mortality. The primary treatment for advanced cancer often includes chemotherapy and radiotherapy, but these approaches have some limitations and pitfalls. Due to the emergence of drug resistance and serious side effects the diseases are not cured properly (Wang et al., 2017). In response, to overcome these shortcomings, scientists have introduced cancer immunotherapy, an innovative approach. It aims to increase the ability of the immune system to attack and degrade cancer cells more effectively. In the last decade, notable developments have been observed in the field of immunotherapy.

Many clinical trials are still under process. However, only a few of these studies have been completed so far. Specific inhibitors for the treatment of distinct types of cancer have been approved. These inhibitors target checkpoint molecules. For example, TIM3, CTLA-4, PD-1, LAG3, PD-L1, and VISTA have changed immunotherapy settings and made them to be used to combat cancer. By blocking the ligand or receptor, the inhibitors can restrict the activation and function of the immune system. The advantage of checkpoint inhibitors used as standard therapy revealed a remarkable outcome in cancer patients (Barbari et al., 2020, Liu et al., 2019).

Moreover, the FDA has approved immune checkpoint blockade therapies for treating several types of tumors. For example, an Ipilimumab, an anti-CTLA4 antibody was approved to treat melanoma (Pediatric, adjuvant). Nivolumab and pembrolizumab are anti-PD-1 antibodies used to treat nonsmall cell lung cancer, Hodgkin lymphoma, and head and neck squamous cell carcinoma. Atezolizumab, avelumab and durvalumab are anti-PD-L1 antibodies for Merkel cell carcinoma urothelial carcinoma, and non-small cell lung cancer (Wei et al., 2018).

Furthermore, the modern study also involves checkpoint agonists (ICOS, OX40, 4-1BB, GITR, CD40) and micro-environment components (IDO or TLR) molecules that target tumor (MarinAcevedo et al., 2018) for therapeutic purposes. In a nutshell, checkpoint blockade not only lead to significant progress in treatment of multiple cancers like non-small cell lung cancer, renal cell carcinoma, small cell lung cancer, head and neck cancer, bladder cancer, gastrointestinal cancer, and lymphomas, but it also could provide potential predictive biomarkers, such as PD-L1 and MSIHi, benefiting patients for cancer diagnosis (Kaufman et al., 2019).

1.8: PD-1-PD-L1 axis

The PD-L1 is an important immune-checkpoint protein with the gene coding located on chromosome 9p24.1. It interacts with the programmed death receptor (PD-1) that is usually expressed on activated T-cells. After such an interaction the T-cell response is attenuated. Basically, inhibiting either PD1 or PDL1 can enhance T-cell responses against cancer. That is considered to be the basis for PD1/PDL1-based immunotherapy, one of the most favorable strategies for treating multiple cancers, including lymphomas (Sun, Mezzadra, & Schumacher, 2018). The programmed cell death protein-1 (PD-1) was first identified in 1992 by TasukuHonjo and his group at Kyoto University. They are also called PDCD1 and CD279. It is a membrane protein consisting of 288 amino acids. It is not only present in different immune cells,like dendritic cells, T-cells, natural killer cells, B-cells, and macrophages, but also other cell types, including microglia and neurons (Ishida et al., 1992).

The PD-1 protein has 50-55 kDa molecular weight. The gene coding belongs to the immunoglobulin gene superfamily. The cytoplasmic tail of PD-1 contains the immune-receptor tyrosine-based inhibitory motif (ITIM), specifically V/IxYxxL. This structure is conserved significantly in mice and humans. The activation antigen is strongly induced in peripheral blood

lymphocytes of both B and T cell lineages (Blank et al., 2005). The PD-1 regulates immune responses negatively. It reduces T-cell activity during immune responses (Salmaninejad et al., 2018). Like CTLA-4, PD-1 interaction with its ligand is crucial for regulating T cell homeostasis. Despite the fact that PD-1 is deficient in the critical MYPPPY motif necessary for binding to B71 and B7-2, but it has distinct binding mechanism that involves its extracellular IgV like domain to interact with PD-L1 and PD-L2. This IgV domain shares 23% structural identity to CTLA-4 (Freeman et al., 2000, Nishimura et al., 1996). The PD-1 possesses two ligands, namely PD-1 ligand 1 (PD-L1 or CD274) and PD-1 ligand 2 (PD-L2 or CD-273) (Dong & Zhang, 2017, Dong et al., 1999).

The PD-1 ligands i.e., PD-L1 and PD-L2 are trans-membrane glycoproteins with type I structure. They possess both IgC and IgV domains. These two ligands share about 40% amino acid similarity. They exhibit only around 20% similarities to B7s and related proteins. Interestingly, human, and murine versions of these ligands show a higher level of identity, which is approximately 70%. An analysis based on crystal structures revealed their binding mechanism. PD-1 interacts by binding with its front beta-face, which comprises the AGFCC' beta-strand. This interaction occurs either with the beta-face of PD-L1 (AGFCC') or the one found in PD-L2 (AGFC). This specific binding interaction regulates the function of the PD-1 pathway in immune responses (Bardhan, Anagnostou, & Boussiotis, 2016). When PD-1 binds to PD-L1 and PD-L2, it suppresses humoral and cellular immune responses. It is found in resting B cells, T cells, macrophages, dendritic cells, and non-immune parenchymal cells like pancreatic cells (non-lymphoid and lymphoid cells) and vascular endothelial cells. In contrast, PD-L2 is specifically induced in dendritic cells and macrophages. The different patterns of expression of PD-L1 and PD-L2 are suggestive of their varying functions depending on cell microenvironment and the specific tissues (Nomi et al., 2007). Disruption of the PD-L1 gene results in the development of self-reactive T-cells and up-regulation of T-cell responses. Blocking either PD-1 or PD-L1 with antibodies enhances anti-tumor immune responses, making it a noble approach for cancer cure (Lin et al., 2008).

1.9: SWI/SNF-type chromatin remodeling complex

Gene transcription regulation through epigenetics involves a series of flexible and dynamic processes managed by complex machinery. In particular, the regulation of euchromatin regions

involves various components, including epigenetic writers like polycomb and trithorax groups, as well as factors such as SWI/SNF complex, which actively modify the chromatin structure (Yamagishi & Uchimaru, 2017).

The DNA tightly coils around a histone protein core within eukaryotic cells, forming nucleosomes, the foundational units of chromatin. The dynamic regulation of nucleosome positioning is deemed crucial in transcriptional control, and subsequently, various biological processes, such as nucleosomes can hinder the binding of transcription factors to DNA. As a result, there is a significant interest in understanding the mechanisms that govern chromatin structure, with the potential to offer insights into regulating gene expression. Chromatin remodeling complexes are crucial in assembling, modifying, and repositioning nucleosomes (Tolstorukov et al., 2013). Moreover, genetic and biochemical investigations have revealed that these complexes can modify nucleosome structure and are ATP-dependent. According to previous studies, these complexes play a pivotal role in the activation of transcription by facilitating the transcription machinery to varying extents. The following five complexes, NURF, SWI/SNF, RSC, ACF, and CHRAC, which are interconnected, fall into this category. These complexes bind the transcription factors to the DNA (Workman & Kingston, 1998).

Chromatin remodeling complexes, which depend on ATP, selectively identify histone marks. By utilizing energy derived from ATP hydrolysis, these complexes uncoil, mobilize, replace, or remove the nucleosome, facilitating the recruitment of a transcriptional apparatus to the nucleosomal DNA. This dual function of chromatin structure serves both as a packaging solution and an intricate mechanism for gene expression regulation. These ATP-dependent chromatin remodeling complexes are huge (> one megadalton) and multi-component, typically ranging from 4 to 17 subunits. The presence of an ATPase component from the helicase superfamily II distinguishes them. These complexes and their subunits exhibit high conservation among eukaryotes (Tang, Nogales &Ciferri, 2010). The extensively investigated ATP-dependent chromatin remodeling complexes are denoted by Switch/Sucrose non-fermenting (SWI/SNF).
The genes encoding SWI/SNF subunits were initially discovered in *S. cerevisiae* by the screening of mutants with alterations in mating-type switching (Switch) and the capacity to grow on nonglucose carbon sources (Euskirchen, Auerbach& Snyder, 2012, Sarnowska et al., 2016). The

primary function of the SWI/SNF complex is to damage nucleosomes and so change the structure of chromatin. This complex is engaged in DNA regions with the help of transcription regulators and other proteins in this process. Once activated the SWI/SNF complex transfers nucleosomes along the DNA strand, altering their location and influencing the accessibility of the underlying DNA sequence. This chromatin reorganization mechanism facilitates gene expression control. When nucleosomes are disrupted, DNA is exposed, allowing regulators to attach to these exposed regions and determine whether a gene is active or silenced. The SWI/SNF complex regulates 6% of the genes in yeast, suggesting its importance in regulating gene expression in these organisms (Savas & Skardasi, 2018).

In-depth biochemical and advanced microscopic studies have confirmed that SWI/SNF remodeling relates to nucleosome sliding and histone-DNA interaction disruption. This opens the chromatin structure, amplifying the binding capacity of transcription factors. The SWI/SNF chromatin remodeling complexes have critical roles in signal transmission, development, and differentiating multi-cellular organisms, as well as DNA methylation directed by RNA. Furthermore, the human SWI/SNF complex is made up of a single ATPase, such as BRM (Brahma) or BRG-1 (Brahma-related gene 1), two SWI-3-type subunits, BAF1-55 and BAF-170, and one SNF-5-type subunit, hSNF-5/IN-I1/BAF-47. Human SWI/SNF complexes also incorporate other 8–10 BAFs (BRM or BRG-1-associated factors). The most interesting is that the specific makeup of the complex varies based on the developmental stage and tissue (Sarnowska et al., 2016). Many SWI/SNF complexes share several key members which are consistently present. These include SMARCB-1 (also recognized and known as (BAF-47, IN-I1, and SNF-5), SMARCC-1/SMARCC-2 also known as (BAF-155 and BAF-170), and one of the two ATPase subunits which are mutually exclusive, either SMARCA-4 (BRG-1) or SMARCA-2 (BRM). These ATPase subunits utilize the energy derived from ATP hydrolysis to facilitate the mobilization of nucleosomes (Alver et al., 2017).

The BRM and BRG1- ATPase subunits are critical components of the SW-I2/SNF-2 family and are crucial to the SW-I/SNF activity. These subunits have similar ATPase and helicase activity and show around 75% structural similarity. These analogies do not mean that their functions are the same. In the human context, BRG1 ATPase can be present in SW-I/SNF CRC classes, i.e.

BAF (BRM or BRG-1 and PBAF (polybromo BRG-1) associated factors. In contrast, BRM is just in the BAF class and is considered a distinctive subunit for this particular complex (Jancewicz et al., 2019). Recent advancements in biochemical analysis, proteomics, three-dimensional structural studies and genetic manipulation have enhanced our understanding of mSWI/SNF complexes. These complexes arose from 29 genes, categorized into three main types: polybromo-associated BAF (PBAF), canonical BAF (cBAF), and noncanonical BAF (ncBAF). The SMARCA4 or SMARCA2 act as mutually exclusive catalytic subunits in each version and comprises common and unique subunits. One important discovery is that SMARCB1 directly interacts with the nucleosome acidic patch, essential for the mSWI/SNF complex's remodeling capability. In addition, the cBAF, PBAF, and ncBAF complexes bind to different chromosomal locations and have different compositions. The presence of either ARID1A or ARID1B, mutually exclusive ATrich interaction domain (ARID)-domain-containing proteins, and the tandem PHD domaincontaining DPF2 subunit, identifies the cBAF complex, which consists of 12 members. On the other hand, the PBAF complex replaces ARID1A/ARID1B with ARID2 and consists of particular elements such as PBRM1, BRD7 (subunits having a bromodomain), and PHF10 (subunit carrying a PHD). A new ncBAF complex with the unusual presence of GLTSCR1/GLSTCR1L and BRD9 subunits was recently discovered; it lacks ARID or tandem-PHD PHF/DPF subunits. These unique mSWI/SNF family complexes attach to various genomic loci and function to maintain and promote DNA accessibility, which controls the transcription of genes (Centore et al., 2020). In addition to these main subunits, the SWI/SNF complex contains between 7 and 15 additional subunits. Recent proteomic analyses revealed additional SWI/SNF subunits such as BCL-7A, BCL-7B, BCL-7C, BCL-11A, BCL-11B and BRD-9 and SYT (SS18).

1.9.1: Mutations in SWI/SNF complex and cancer

Somatic mutations affect chromatin and several related epigenetic processes of DNA modification. These mutations include genes that code for the enzymes responsible for histone transformation, like CREBBP, EP-300, KDM-6A, EZH-2, SUZ-12 and MLL. Additionally, mutations affect enzymes involved in DNA methylation or hydroxylation, like DNMT-3A, TET-1, and TET-2, as well as histones such as H3F-3A and HIST1H-3B. Mutations in at least one gene in 59% of bladder tumours are responsible for enzymes engaged in epigenetic gene regulation. These genes are KDM-6A, MLL, MLL-3, CREBBP, EP-300, ARID1A, and CHD-6.

Chromatin remodeling has generated considerable interest in the various alterations in epigenetic processes. Extensive research shreds of evidence that SWI/SNF complexes undergo alterations in numerous cancer types, making the genes responsible for chromatin remodelers among the most commonly mutated epigenetic regulators in cancer.

It was revealed 15 years ago that SWI/SNF complexes are involved in tumour formation through somatic truncating mutations in the SMARCB-1 gene (hSNF5, INI1) in malignant rhabdoid tumours (MRTs). Afterwards, germline mutations in the SMARCB-1 gene have been linked to MRT predisposition syndrome. Inclusive genomic analyses across various tumour types have revealed gene mutations related to the SWI/SNF complex, which cause tumours. In about 20% of all human tumours, these mutations are detected. The mutation frequency impacting genes that encode SWI/SNF subunits is comparable to that of TP-53, KRAS, or PTEN, the most commonly mutated tumour suppressor genes and oncogenes. Consequently, the SWI/SNF complex dysfunction significantly contributes to carcinogenesis (Masliah-Planchon et al., 2015).

The INI1, one of the most widely recognized subunits associated with tumour suppression, plays a critical role in inhibiting the development and advancement of malignant rhabdoid tumour of childhood (MRT). Mutations such as deletions, nonsense mutations and frameshifts in the gene encoding INI1 (BAF47, hSNF5, SMARCB1) are common and lead to the initiation and progression of MRT (Versteege et al., 1998). In addition, mutations of single-residue in the Cterminal domain of SMARCB-1 have also been identified in tumour such as meningiomas, adenocarcinomas, and schwannomas (Valencia et al., 2019). Other tumours, such as renal cell carcinoma (RCC), commonly lack BRM expression (Xia et al., 2014).

Loss of BRG1 and BRM subunits (BRG1/BRM) has been reported in approximately 30% of nonsmall cell lung tumours and shows a relationship with poor prognosis (Reisman et al., 2003). Similarly, loss of SMARCA4 protein was also observed in small cell ovarian carcinoma of hypercalcemic type (SCCOHT) (Ramos et al., 2014). The ARID-2 is thought to regulate epigenetic changes. ARID2 mutations are common in hepatocellular carcinoma (HCC), often resulting in partial or complete inactivation of ARID2 protein function (Jiang et al., 2020). In addition, somatic mutations of chromatin remodeling factors such as ARID1A, SMARCA2, and SMARCA4 have been identified in 30% of gastric cancer (Takeshima et al., 2015).

Recent studies have identified novel functions of SWI/SNF components in regulating antitumor immunity. Furthermore, targeted treatment of SWI/SNF deficiency by blocking immune checkpoints (ICBs) has emerged as a potential therapeutic approach. These findings highlight the importance of the SWI/SNF complex as a predictive biomarker for the satisfaction of the patients and predicting response to ICB treatment (Zhou et al., 2021). Deficiency of SMARCA4 has been observed in association with an improved response to immune checkpoint blockade (ICB) treatment. In a previous study in which (n=126) patients with squamous-cell carcinoma of the head and neck received anti-PD-1/L1 therapy, a higher prevalence of SMARCA4 mutation was observed in patients with a positive response to treatment compared to non-responders (Hanna et al., 2018).

1.10: EZH2, an epigenetics modifier

The EZH2 (Zeste homolog two enhancers) is an essential epigenetic regulator, a crucial polycomb repressive complex-2 (PRC-2) member. It helps in controlling gene expression through H3K27me3. It has dual functionalities, i.e., it may function as a transcription coactivator or repressor, depending on the condition of the cell. It is associated with cancer because it affects the expression of vital genes involved in invasion, drug resistance, cell proliferation and cell survival. Even the dysregulation of EZH2 is also reported in different types of cancer at the genetic, transcriptional, and post-transcriptional levels, thus contributing to tumour development. Furthermore, the *EZH2* gene was evolutionary conserved among other species (Gan et al., 2018). The presence of elevated levels of EZH2 in cancerous tissues is notable in cancerous tissues compared to their corresponding healthy ones. Increased level of EZH2 expression correlates not only with the advanced stages of the disease but also with a more unfavorable prognosis (Karantanos et al., 2016). Abnormal over-expression of EZH2 was observed in breast cancer (Kleer et al., 2003), bladder cancer (Weikert et al., 2005), melanoma (Bachmann et al., 2006), and gastric cancer (Matsukawa et al., 2006). Moreover, somatic point mutations in EZH2 have also been found in diffuse large B-cell lymphoma (22%) and follicular lymphoma (7–12%). These mutations mainly occur in Y641 in the SET catalytic domain of C-terminus (Yamagishi and Uchimaru, 2017), (Morin et al., 2010).

Current studies not only revealed the involvement of EZH2 in cancer development but also made it one of the exciting targets for anticancer treatments (Karantanos et al., 2016). For instance, suppression of EZH2 increased the immune response to chordomas (a rare bone tumour) missing the SMARCB1 subunit (Gounder et al., 2019).

The EZH2 is considered to be a target for therapy to restore the proper equilibrium of epigenetic regulation when there is an abnormal gain in its expression or activity using upregulation (silencing of genes that lead to oncogenesis) and mutation (in catalytic SET domain) or loss of function in antagonistic molecules (e.g., KDM6A or BAP1) (Yamagishi, &Uchimaru, 2017).

2. SCOPE AND OBJECTIVES OF THE STUDY

The immune checkpoint proteins, with PD-L1 as a good example, could be utilized in cancer immunotherapy, as reported for several types of malignancies. Considering its potential benefits for cancer treatment the present study was conducted to better understand the molecular mechanism of PD-L1 action and its regulation in classical Hodgkin lymphoma. Moreover, the immune system complexity and diversification of cancer cells leads to many obstacles to target this check point. So, it's crucial to understand its regulation and signaling pattern. Therefore objectives of current study were as follows:

1. Understanding the mechanism of CD274 gene encoding PD-L1 overexpression on promoter regulation level;
2. The function of PD-L1 protein in HRS cells.

3. MATERIALS AND METHODS

3.1: Buffers and solutions

All buffers mentioned below were prepared from chemicals available in the laboratory of the Department of Experimental Immunotherapy.

- **Buffer for agarose electrophoresis** (TBE): 89 mM Tris/borate pH 8.3, 89 mM boric acid, 2 mM EDTA, ethidium bromide 0.5 μg/ml
- **SDS-PAGE electrophoresis buffer:** 25 mM Tris-HCl pH 8.3; 192 mM glycine, 0.1% SDS
- Transfer buffer after SDS-PAGE: 0.05 M Tris-HCl, 0.05 M boric acid.
- **Buffers for ChIP protocol:**

o Lysis buffer: 10 mM Tris-HCl pH 7.5, 150 mM NaCl, 0.5 mM EDTA, 1% Triton X-100, 0.5 mM DTT, 1x PiC, 1 mM PMSF

o Wash buffer: 10 mM Tris-HCl pH 7.5, 150 mM NaCl, 0.5 mM EDTA, 1x PiC, 1 mM PMSF.

o Elution buffer: 10 mM Tris-HCl pH 7.5. 300 mM NaCl, 1% SDS

- **Laemmli Buffer** (lysis buffer for material destined for SDS-PAGE): 0,25% bromophenol blue, 0.5 M DTT, 50% glycerol, 0.25 M Tris-HCl pH 6.8; 10% SDS.
- **PBS** (phosphate buffered saline), 0.14 M NaCl, 2.7 mM KCl, 10 mM Na2HPO4; 1.8 mM KH2PO4, pH 7.3.
- **RIPA**: 10 mM Tris-HCl pH 7.5, 150 mM NaCl, 2.5 mM MgCl2, 1% sodium deoxycholate, 1% Triton X-100, 0.8% SDS, 0.5 mM EDTA, 1x PiC, 1 mM PMSF, 0.5 mM DTT
- **TBS** (Tris buffered saline): 150 mM NaCl, 50 mM Tris-HCl, pH 8.0.
- **TBS-T**: 150 mM NaCl, 50 mM Tris-HCl pH 8.0, 0.1% Tween-20
- 5% milk in TBS-T. 5% of
- **Tris-HCl** of appropriate molarity (0.5 M, 1 M, and 1.5 M) with appropriate pH (8.8, 8.0, 7.5, 6.8) adjusted with HCl.
- **DNA Gel Loading Dye** Cat. NO. R0611, Thermo Scientific™
- **Polyacrylamide gel separating:**

- 10 ml (adjusted with ddH_2O) 10% polyacrylamide separating gel: 2.5 ml 40% acrylamide/bis-acrylamide (29:1), 2.5 ml 1.5 M Tris-HCl pH 8.8, 100 µl 10% SDS, 0.5% TCE, and polymerization catalysts: 50 µl 25%APS, 8 µl TEMED.
- 10 ml (adjusted with ddH_2O) 12% polyacrylamide separating gel: 3 ml 40% acrylamide/bis-acrylamide (29:1), 2.5 ml 1.5 M Tris-HCl pH 8.8, 10% SDS, 0.5% TCE, 50 µl 25% APS, 8 µl TEMED.

- Polyacrylamide gel thickening 5%, 5 ml (adjusted with ddH_2O):
  - 625 µl 40% acrylamide/bis-acrylamide (29:1), 1.25 ml 1M Tris-HCl pH 6.8, 50µl 10% SDS, (polymerization catalysts: 13.5 µl 25% APS, 3 µl TEMED)
  - N, N,N',N'-tetramethylethylenediamine (TEMED), Cat. No. 161-0800, Bio-Rad
  - 2,2,2-Trichloroethanol (TCE), Cat. No. T54801, Merck (Sigma-Aldrich)
- **Ready-to-use reagent kits**
  - Agarose-Out DNA Purification Kit (Agarose gel purification kit), E3540, EurX
  - DNA Purification Buffer and Spin Columns, ChIP, CUT&RUN (kit for DNA isolation and immunoprecipitation kit), cat. no.14209S, Cell Signaling Technology
  - Monarch® Plasmid Miniprep Kit (kit for isolation of plasmid DNA from a volume of 1-5 ml), Cat. No. T1010, New England BioLabs
  - PureYield™ Plasmid Midiprep System (plasmid DNA isolation kit from volumes of 50-200 ml), Cat. No. A2495, Promega
  - EndoFree® Plasmid Maxi Kit (plasmid DNA isolation kit, large scale), Cat. No. 12362, Qiagen
  - ReliaPrep™ RNA Cell Miniprep System (RNA isolation kit), Cat. No. Z6011, Promega
  - Transcriptor First Strand cDNA Synthesis Kit (cDNA synthesis kit on matrix RNA), Cat. No. 04896866001, Roche Diagnostics
  - Western Bright™ Quantum (chemiluminescent substrate for HRP), Cat. No. K-12042-D20, Advansta
- **Size standards/Markers**
  - Protein size standard: Precision Plus Protein™ Dual Color Standards, Cat. No.1610374, Bio-Rad
  - Nucleic acid size standard: 1 kb DNA Ladder RTU, Cat. No. SD010-R600, Gene Direx
  - Lambda DNA/EcoRI plus HindIII Marker Cat No. SM0191, Thermo Scientific™
- **Antibiotics**
  - Carbenicillin in powder form, Cat. No. J61949.03, VWR International Ltd.
- **Enzymes**

- **Restriction nucleases:**
  - *Bam*HI, Cat. No. FD0054, (Fast digest) ThermoFisher Scientific
  - *Eco*RI, Cat. No. FD0274, (Fast digest) ThermoFisher Scientific
  - *Sal*I, Cat. No. FD0644, ThermoFisher Scientific
- **DNA Ligases:**
  - T4 ligase, Cat. No. M0202, New England Biolabs
- **Polymerases:**
  - AccuPrime™Taq DNA polymerase, High Fidelity, Cat. No. 12346, Thermo Fisher Scientific (Invitrogen)
  - iQ™ SYBR® Green Supermix, Cat. No. 1708886, Bio-Rad
  - SapphireAmp® Fast PCR Master Mix, Cat. No. RR350A, TaKaRa

Other enzymes:

- OMNI Nuclease, Cat. No. E1120, EurX
- Proteinase K (20 mg/ml), Cat. No. AM2546, ThermoFisher Scientific (Ambion)
- PureLink™, RNase A (20 mg/ml), Cat. No. 12091021, ThermoFisher Scientific

- **Antibodies**

Abbreviations used in the section: mAb: monoclonal antibody, pAb: polyclonal antibody, Co-IP: co-immunoprecipitation, ICC/IHC: immuno-cytochemistry/immune-histochemistry, IF: immune-fluorescence, WB: Western Blot, ChIP: Chromatin immune-precipitation. Working dilutions given in brackets.

- **Primary antibodies:**
  - Anti-BAF155, clone D7F8S, rabbit mAb, Cat. No. 11956, Cell Signaling Technology (WB: 1:1000, ICC/IHC: 1:200, IF: 1:50)
  - Anti-BRM, clone D9E8B, rabbit mAb, Cat. No. 11966, Cell Signaling Technology (WB: 1:1000, ICC/IHC: 1:200, IF: 1:50)
  - Anti-EZH2, clone D2C9, rabbit mAb, Cat. No. 5246, Cell Signaling Technology (WB: 1:1000)
  - Anti-Histone Tri-Methyl-Histone H3 (Lys27), clone C36B11, rabbit mAb, Cat. No. 9733, Cell Signaling Technology (ChIP: 1:50)
  - Anti-histone Acetyl-Histone H3 (Lys27), clone D5E4, rabbit mAb, Cat. No. 8173, CellSignaling Technology (ChIP: 1:20)

- Anti-IgG rabbit pAb, Cat. No. 2729, Cell Signaling Technology (Co-IP 1:20)
- Anti-INI (SNF5/BAF47), clone D9C2, rabbit mAb, Cat. No. 8745, Cell Signaling Technology (WB: 1:1000, IHC/ICC: 1:200)
- Anti-PD-L1, clone E1L3N®, rabbit mAb, Cat. No. 13684, Cell Signaling Technology (WB: 1:1000)

- **Secondary antibodies:**

o Anti-rabbit IgG ImmunStar™, HRP-conjugated, goat pAb, Cat. No. 170-.5046, Bio-Rad (WB: 1:10000)

o Anti-rabbit IgG, conjugated to Alexa Fluor 594, goat pAb, Cat. No. ab150080, Abcam (IF: 1:1000)

- **Magnetic beads**

o Pierce™ Protein A Magnetic Beads, Cat. No. 88846, Thermo Fisher Scientific

o Protein G substrate: Protein G Magnetic Beads, Cat. No. 70024, Cell Signaling Technology

- **Antibodies for flow cytometry:**

o CD3-APC mouse-anti human, clone SK7, Cat. No. 345767, Becton Dickinson

o PD-1 (CD279)-PE anti-human; Cat. No. 555749, BD Pharmingen

o PD-L2 (CD273)-APC anti-human, Cat. No. 557926, BD Pharmingen

o PD-L1 (CD274)-PE anti-human, Cat. No. 557924, BD Pharmingen

o 7- AAD Cat. No. 559925, BD Pharmingen

- **Fluorogenic dyes for confocal microscopy**

o MitoSOX Red: (Excitation/Emission) ~396/610 nm, Cat. No. M36008, Thermofisher, USA

o Hoechst 33342, Trihydrochloride, Trihydrate, Cat. No. H1399, Thermofisher, USA

o Calcien AM, Cat. No. C3099, Thermofisher, USA

- **Primers for CHIP q-PCR:**

Table 3. 1: Sequences of primers used in CHIP q-PCR.

CD274_1	5'-CTAGAAGTTCAGCGCGGGAT-3'	5'-GGCTGCGGAAGCCTATTCTA-3'
CD274_2	5'-TTCCGCAGCCTTAATCCTTA-3'	5'-CGTGGATTCTGTGACTTCCTC-3'
CD274_3	5'-	AAAGTCAGCAGCAGACCCATA-

	CGAGGAACTTTGAGGAAGTCA-3’	3’
CD274_4	5’-ATGGGTCTGCTGCTGACTTT-3’	5’-ACCTTCAGAGGGGTAAGAGC-3’
CD274_5	5’-ACCCCTCTGAAGGTAAAATCAA-3’	5’-ACCCCTCTGAAGGTAAAATCAA-3’
CD274_6	5’-TTCCCGGTGAAAATCTCATT-3’	5’-TCCTGACCTTCGGTGAAATC-3’
CD274_7	5’-CGAAGGTCAGGAAAGTCCAA-3’	5’-GAAGCTGCGCAGAACTGG-3’
CD274_8	5’-CAGTTCTGCGCAGCTTCC-3’	5’-GACCCTCCGTCCTAAAGTGC-3’
CD274_9	5’-TAGCTCGCTGGGCACTTTAG-3’	5’-CAGATGCATTGCCTGTTCTT-3’
CD274_10	5’-AATGCATCTGGCCTTCCTC-3’	5’-TGAACACACAGTCGCATAAGAA-3’
CD274_11	5’-TGCGACTGTGTGTTCAGAAT-3’	5’-ATGCTGCAGCTGGGATAACT-3’

- **Primers for cloning:**

Table 3.2: Sequences of primers used in cloning of PD-L1 and FUS cDNA.

Gene		Sequence
Forward	PDL1FE	GCGGAATTCAGGATATTTGCTGTCTTTATATTC
Reverse	PDL1RSS	CGCGTCGACGGTGCTAGGGGACAGTG
Reverse	PDL1RSL	CGCGTCGACCGTCTCCTCCAAATGTG
Forward	FUS-F	GCAGGATCCGTATGGCCTCAAACGATTATACCCAAC
Reverse	FUS-R	GCGGTCGACTTAATACGGCCTCTCCCTGCGATCC

- **Primers for q-RT PCR:**

Table 3.3: Primers used in q-RTPCR for analysis of expression of genes as mentioned below.

Gene	Forward primer sequence	Reverse primer sequence	Type
UBC	ATTTGGGTCGCGGTTCTTG	TGCCTTGACATTCTCGATGGT	**Reference gene**
SMARCA2 / BRM	TCCGAGGCAAAATCAGTCAAG	TTCCTCGATTTGGCCTTTTCT	**SWI/SNIF complex**
SMARCA4 / BRG1	GACATTCCAGTCTCGACCCC	GCAACAGTACTGCCAGCAAC	
SMARCC1 / BAF155	ACTTGTAAGCAGCCCCAAGA	GCAGCTTCTTCAGTTCCAGG	
SMARCC2 / BAF170	ACAGACATCACCCGCTAGGT	ACGGCAAGAACAAGTCCAAG	
EZH2	GAACCTCGAGTACTGTGGGC	ACACTTTGCAGCTGGTGAGA	**PRC complex**

- **Media:**
- **Cell culture media**
  - Fetal Bovine Serum (FBS), Cat. No. S1810-500, Biowest
  - RPMI 1640 W/ stable glutamine, Cat. No. L0498-500 Biowest
- **Bacterial culture media**
  - LB liquid medium: Cat. No. L3022-1KG, Merck (Sigma-Aldrich)
  - LB agar medium (solid): Cat. No. L2897-1KG, Merck (Sigma-Aldrich)

Other reagents and materials:

- Dimethyl sulfoxide (DMSO): Cat. No.62247, Merck (Sigma-Aldrich)
- Ditiotreitol (DTT): Cat. No. 0281, BioShop
- GlicerolCat. No. G5516, Merck (Sigma-Aldrich)
- Methanol Cat. No. 176840010, Acros organics
- PVDF membrane: Immobilon P, Cat. No. IPVH00010, Merck Millipore

- Chromatography paper: Whatman 3MM Chr, Cat. No. 3030-672, GE Healthcare LS
- Powdered milk for Western Blot: Skim milk, Cat. No. LP0031, Oxoid

- **Bacterial strains**

- *Escherichia coli* DH5α: Genotype, F – φ80lacZDM15 D(lacZYA-argF) U169 recA1 endA1 hsdR17 (rk–, mk+) phoA supE44 l – thi–1 gyrA96 relA1

- **Yeast strain for two hybrid system**

- Y190: Genotype, MATa ura3-52 his3-200 lys2-801 ade2-101 trp1-901 leu2-3, 112 gal4Δ gal80Δ LYS2::GAL1UAS-HIS3TATA-HIS3, URA3::GAL1UAS-GAL1TATA-lacz

- **Positive control for Y2H**

- pCL1: GAL4 2H & 2H-2 wild-type full-length GAL4 –gene in a YCp50 derivative, LEU2, ampr

- **Yeast culture media**

- YPD medium with agar, cat. no.: Y1500-1KG, Merck (Sigma-Aldrich)
- Yeast Nitrogen Base without aminoacids, Cat. No. Y0626, Merck (Sigma-Adlrich)
- SD-L-W medium with agar: 0.67% basic yeast medium; 0.14% synthetic yeast dropout Cat. No. Y2001-20G, Merck Life Science, 20% D-glucose, Cat. No. G8270, Merck (Sigma-Aldrich), 2% histidine, Cat. No. H8000-100G, Merck Life Science, 2% uracil Cat No. U0750-100G, Merck Life Science, 2% agar, prepared and autoclaved.
- SD-W medium with agar: 0.67% basic yeast medium; 0.14% synthetic yeast dropout; 20% D-glucose; 2% histidine, 2% uracil, 2% leucine Cat. No. L8000-100G, Merck Life Science, 2% agar, prepared and autoclaved.
- SD-L medium with agar: 0.67% basic yeast medium; 0.14% synthetic yeast dropout; 20% D-glucose; 2% histidine, 4% tryptophan Cat. No. T3300-100G, Merck Life Science, 2% uracil, 2%, prepared independently and autoclaved.

- **Plasmids used in the yeast two-hybrid assay**

- pGAD424: a commercially available plasmid that allows expression of the investigated protein as a hybrid with a yeast Gal4 activation domain protein (Gal4AD) at the C-terminus of this domain, used in a yeast two-hybrid assay. It has an ampicillin resistance gene and a LEU2 gene, part of the pathway for synthesis of leucine, used for yeast selection.
- pGAD424-PD-L1 (V1): a vector based on the pGAD424 plasmid with PD-L1 coding sequence (cds) in fusion with GAL4 activation domain. It encodes ampicillin resistance and the LEU2 gene as well.

(V1: Large Isoform of PD-L1, 885 bp)

- pGAD424-PD-L1 (V4): a vector based on the pGAD424 plasmid with PD-L1 V4. It also encodes ampicillin resistance and the LEU2 gene.

(V4: Short Isoform of PD-L1, 750 bp)

- pGAD424-BAF155: a vector based on the pGAD424 plasmid with SMARCC1 cds. It encodes ampicillin resistance and the LEU2 gene.
- pGAD424-SNAIL: plasmid-based vector pGAD424 with SNAI1 cds. It encodes bacterial ampicillin resistance and the LEU2 gene.
- pGAD424-SLUG: a vector based on plasmid pGAD424 with the SNAI2 cds. It encodes bacterial ampicillin resistance and the LEU2 gene.
- pGBT9; a commercially available plasmid that allows expression of the investigated protein in fusion with yeast GAL4 protein binding domain (Gal4BD) at the C-terminus of this domain, used in the yeast two-hybrid assay. It has a gene ampicillin resistance and the TRP1 gene, which is part of the tryptophan synthesis pathway, used in yeast selection.
- pGBT9-PD-L1 (V1): a vector based on the pGBT9 plasmid with PD-L1 cds, variant V1 (see above, pGAD424-PD-L1 V1). It encodes ampicillin resistance and the TRP1 gene.
- pGBT9-PD-L1 (V4): a vector based on the pGBT9 plasmid with PD-L1 cds, variant V4. It encodes ampicillin resistance and the TRP1 gene.
- pGBT9-AMPKα1: a vector based on the pGBT9 plasmid with AMPKα1 cds. It encodes the bacterial ampicillin resistance and TRP1 gene.
- pGBT9-SNAIL: a vector based on pGBT9 plasmid with SNAI1 cds. It encodes gene resistance to ampicillin and the TRP1 gene.
- pGBT9-SLUG: a vector based on plasmid pGBT9 with the SNAI2. It encodes resistance to ampicillin and the TRP1 gene.
- pGBT9-BAF155: a vector based on pGBT9 plasmid with the BAF155(SMARCC1) cds. It encodes gene resistance to ampicillin and the TRP1 gene.

- **Chemicals of MTT test**
  - MTT – 3-(4,5-dimethylthiazol-2-yl)-2,5-diphenyltetrazolium bromide or thiazolyl blue tetrazolium bromide, M5655, Merck (Sigma-Aldrich).
- **Epi drug/EZH2 inhibitor with K_i=2.5nM**
  - Tazemetostat (EPZ-6438) Cat. No. S7128, Selleck USA

- **Hodgkin lymphoma cell lines**
  - L-1236 (ACC530)
  - L-428 (ACC197)
  - KM-H2 (ACC8)

They have been verified by Eurofins Genomics GmbH, Germany.

Equipment

• Neubauer hemocytometer (counting chamber), improved

• Incubators:

- PHCBIMCO-170AICUV CO2 Incubator, Panasonic,
- MaxQ™ 6000 Incubated/Refrigerated Stackable Shakers, Cat. No. SHKE6000, Thermo Scientific
- Confocal microscope: ZEISS LSM 800, with fluorescence module and chamber maintaining a constant temperature and CO_2 level during observations.
- Inverted light microscope: Opta-tech MW50 with MI20 camera.
- Chemiluminescence and fluorescence imaging platform: Amersham™ ImageQuant™ 800 biomolecular imager
- BD FACS Aria™ Cell Sorter, Model No.648282-20

• Centrifuges:

o MiniSpin®, Eppendorf,Cat No. 5452000010

o Centrifuge 5424R, Eppendorf,Cat No. 5420000318

o Sorvall® RC 5B Plus, Marshall Scientificabout MPW-350R

• Spectrophotometer: NanoDrop™ 2000, ThermoFisher

• Thermoblocks:

o ThermoMixer® F1.5, Eppendorf

• Thermal cyclers:

o Mastercycler® Nexus, Eppendorf

o Mastercycler® Nexus X2e, Eppendorf

o 7500 Fast Real-Time PCR, Applied Biosystems™

o CFX384 Touch™ Real-Time PCR Detection System, Bio-Rad

• Electrophoresis devices:

o Horizontal: multiSUB Mini, Celaver Scientific

o Vertical: Mini-PROTEAN® System

Methodology

3.2: Cell culture

Cells were cultured as three different cell lines in dedicated media i.e. RPMI 1640 medium with the addition of 10% FBS, without antibiotics. All cell lines were cultured in an incubator at 37°C, 5% CO_2 and 100% humidity.

3.2.1: Thawing, culturing and freezing of cell lines

The selected cell lines (KM-H2, L-1236, and L-428) were thawed from the cell bank of the Department of Experimental Immunotherapy at the Maria Sklodowska-Curie National Research Institute of Oncology in Warsaw. The thawing process involved removing the freezing tubes, incubating them for 10 minutes, and then centrifuging at room temperature (RT) at 600 rpm for 5 minutes to remove traces of DMSO. The resulting cell pellet was suspended in 3-5 ml of a dedicated medium and incubated under standard conditions.

After thawing, the cell lines were cultured for 2-3 passages before the planned experiment. The passage intervals varied depending on the cell line, typically occurring every 48-72 hours. The decision to perform a passage was based on observed indicators such as the medium color turning yellow or the growth reaching its optimal density. The harvested cells were then subjected to further analyses.

Table 3.4: Hodgkin cell lines with their respective optimal growth density and cell doubling time.

Cell line	Density	Division rate/time
L-428	0.2-0.5× 10^6	35 h
L-1236	0.3-0.5 × 10^6	48 h
KM-H2	0.2-1.0 × 10^6	48 h

3.3: Vertical denaturing polyacrylamide gel electrophoresis (SDS-PAGE)

Vertical electrophoresis in a polyacrylamide gel also called SDS-PAGE was performed and then the gel analyzed by the Western blot. For this procedure, 5% thickening gel also known as stacking gel with pH 6.8 and 10% or 12% separating gel also termed as resolving gel with pH

8.8were used. Moreover, for protein visualization trichloroethanol (TCE) 0.5% (final concentration) was added to the separating gel prior to electrophoresis (Ladner et al., 2004).

Protein extract, obtained from 1-5 x 10^6 cells, was suspended in 200 µl of 1x Laemmli Buffer and incubated at 95°C for 10 min in thermal block. After that, 10^{th} / 20^{th} parts of the resulting lysates (~ 20µl each) along with Protein standard marker were loaded to the gel. Electrophoresis was performed in a vertical electrophoresis apparatus in running buffer under constant current, usually 25 mA for 1-1.5 hours depending on percentage of the separating gel. Bands after electrophoretic separation were visualized using a UV trans- illuminator or gel doc system.

3.3 .1: Western Blot

Protein transfer from a gel to a Polyvinylidene difluoride (PVDF) membrane with a pore size of 0.45 µm was carried out in a transfer buffer at a constant voltage of 12 V for overnight. Then, using UV light, the bands on the membrane were visualized and documented as sample loading control. After that, membrane was subjected to blocking for 1 hour at RT, using a solution of 5% skimmed milk in TBS-T buffer. Then the membrane was incubated overnight at 4°C with primary antibodies specific for the antigen (e.g. anti PD-L1, BRG1, INI1, BAFF155, EZH2 and CD30). The antibodies were suspended at an appropriate dilution (1:1000 in most cases) in 5% milk or 5% BSA in TBS-T, depending on the manufacturer's instructions. On the next day, membranes were washed 3 x 5 min at RT in TBS-T buffer and then incubated with the appropriate HRP-conjugated secondary antibody (1: 10,000 dilution) suspended in 5% milk in TBS-T at least for an hour. The membrane was then washed again three times in TBS-T for 5 minutes.

After washes, the substrate for horseradish peroxidase was applied to the membrane (Western Bright™ Quantum), causing chemi-luminescence. Then, chemi-luminescence signal was collected and documented using an appropriate camera and gel doc system.

3.4: Isolation of cellular nucleus or nuclear fraction

Almost 5x 10^6 frozen cells were suspended in Extraction buffer (2 x M2EB) with 20% glycerol, 1M DTT, 10µl/ml PIC (protease inhibitor cocktail), and PMSF (phenyl-methyl-sulfonyl fluoride) on ice. Cells were homogenized by glass homogenizer and filtered by double layer of Miracloth tissue. The filtrate was centrifuged for 10 minutes, at 2000 rpm at 4 °C. The supernatant

contained cytoplasm while the bottom pellet comprised of nucleus fraction. The pellet was diluted by adding 50 µl of above-mentioned Extraction buffer (2 x M2EB) and 5 x Laemmli buffer. It was further subjected for the Western blot analysis with Histone 3 used as a positive control.

3.5: Confocal Microscopy

Up to 5x10^6 cells were transferred to the one well of a 6-well plate. Then they were centrifuged at 1200 rpm for 5 minutes. The medium was replaced with a fresh one containing 50nM CMXRos Mitotracker Red (for mitochondria) and 4uM Calcein AM (for cell viability) fluorescent dyes. Cells were incubated at 37°C and 5% CO_2 for 30mins.Then cells were washed 3 times with PBS, re-suspended in PBS containing 4% formaldehyde and incubated RT for 15 minutes at room temperature. After incubation they were washed again with PBS (3 times), re-suspended in PBS containing 10uM Hoechst (for nucleus) and incubated for 5 minutes. After washing again, the cells were re-suspended in 400uL of PBS and then transferred to a chamber cover glass and finally were observed under a microscope.

3.6: Immuno-precipitation (IP)

Cellular nuclei pellet was isolated for L1236 cell line by applying the nuclear fraction protocol. After that the cell lysate was re-suspended in 500 µl RIPA buffer, supplemented with PMSF (1: 200, usually 5 µl) and PIC (1:100). DNase I, RNase or Omni Nucleases (5µl) were used to digest nucleic acid, centrifugation was done 10,000-12,000 rpm for 10 minutes, at 4 °C. The 1/10th of supernatant was separated and considered as “input”. The rest of supernatant was divided in to two parts, one for IgG as a control and the other one for anti-PD-L1 IgG. In each respective tube (5µl) of IgG and anti-PD-L1 IgG against specific protein was added, gently shaken and incubated for overnight at 4 °C on a rotator. The next day, Dyna beads (magnetic beads) with protein A (20 µl) were added and incubated for 1-3 hours, 4°Cwith mixing.

After incubation with magnetic beads, the supernatant was washed three times with RIPA buffer at 4°C. While at final rinse 1/10th of the sample was transferred to a new tube along with beads. The remaining amount of supernatant with magnetic beads was sent for Mass spectrometric analysis to the Institute of Biochemistry and Biophysics of the Polish Academy of Sciences (Warsaw, Poland).

The next step, supernatant was removed carefully from the tubes with 1/10th sample and beads on a magnetic stand. The beads were re-suspended in 50 µl of 1x concentrated Laemmli buffer along with the previously collected "input" and IgG control samples and then boiled at 95°C for10 minutes in a water bath. The beads were then pulled down back on a magnetic stand and supernatants loaded onto an SDS-PAGE gel and analyzed by Western blot.

3.7: Chromatin immune-precipitation (ChIP)

Chromatin immune-precipitation (ChIP) was performed to check the interaction of protein with DNA. The cells were cultured under standard conditions, almost $2x10^6$cellsfor one antibody were used. Here a total of $12x10^6$cells for 6 antibodies were used. The experiment was performed with anti-IgG, anti-BAF 155, anti-PD-L1, anti-EZH2, anti-K27ac andanti-H3 K27me3 antibodies. All steps were performed at 4°C, and incubations were carried out by using orbital shaker with constant mixing. The experiment was repeated 3 times.

The cell pellet was re-suspended in cold PBS. Subsequently, the cells were fixed in 1 mM BS2G for 20 minutes and then in 37 % formaldehyde for 10 minutes. In order to stop the cross-linking reaction, 100 mM glycine was added for 5 minutes. The solid cells suspension was centrifuged at 500 x g for 5 minutes. The cells were then washed two times with PBS, incubated for 5 minutes each time, and centrifuged again.

After that, the next day, the cells were lysed in lysis buffer for 15 minutes and centrifuged at 2000x g for 5 minutes. This step was repeated twice. Almost for each antibody $2x10^6$ cells were resuspended in 600 µl of RIPA buffer and incubated for 30 minuteson orbital shaker. Each sample was then sonicated 5 times for 10 minutes (30 seconds sonication, 30 seconds pause, sonicate conditions: High) with at least a 2-minute interval between sonications. After this step, the samples were treated with7.5 µl RNAse (10 mg/ml).25 µl of each DNA probe for chromatin sonication was checked. The sonicated chromatin was further treated with 6 µl of 5 M NaCl and 2 µl of Proteinase K, incubated at 65°C overnight.

The sonicated material should not contain DNA fragments longer than 500 base pairs. The correctness of the sonication was checked by isolating DNA from samples with a ChIP reagent kit from CST. Each sample was then incubated with the appropriate antibodies (anti-IgG, BAF 155, PD-L1, EZH2, H3 K27ac and H3 K27me3) at a dilution of 1:200 (usually 5 µl) over night at

4°C on an orbital shaker. The next day (3rd day of an experiment), 30 µl of the mixture was added to the magnetic beads with embedded proteins A and G (1:1 proportion) and incubated for 2 hours.

After incubation, the magnetic beads were washed three times with a washing buffer. The buffer in the last rinse did not contain protease inhibitors and PMSF. Elution was conducted in 270 µl of elution buffer with 10% SDS at 65°C overnight. After that 5µl of Proteinase K was added at a concentration of 0.3 mg/ml and incubation was continued for 2 hours at 55°C. Next day (4thday of an experiment), the sample mixture was precipitated by following the phenol/chloroform/isoamyl alcohol (25:24:1) method to extract and precipitate the DNA. The above-mentioned reagent was added to each mixture, samples centrifuged, and then chloroform added to the aqueous phase and centrifuged 13 800 x g, RT, 5 min. again. The aqueous (upper) phase was transferred to new tubes. 1/10th of the sample volume of glycogen (1 µl) and3 M sodium acetate (pH 5.2) and 2.5 volumes of 96% ethyl alcohol were added and incubated for at least 1 hour at -80°C overnight to precipitate the DNA. The mixture was centrifuged at maximum speed (14000 rpm) for 15 min at 4°C.After that the supernatant was discarded and nucleic acid pellet was washed with 70% cold (-20°C) ethyl alcohol and centrifugation were done again. The supernatant was discarded, and the pellet was allowed to completely dry at RT. DNA was dissolved in 30 µl of nuclease-free water and its concentration was measured by using a NanoDrop™ 2000 spectrophotometer. DNA was then diluted to a final concentration of 1 ng/µl. The obtained nucleic acid was used for qPCR reactions with primers specific to the PD-L1 gene promoter. It can be stored at -20°C for three months maximum.

3.7.1: Quantitative polymerase chain reaction (q-PCR)

Quantitative polymerase chain reaction (q-PCR) is a sensitive technique used for the amplification and detection of the gene of interest as well as any segment of DNA. This technique usually includes the fluorescent dye (like the SYBR Green) that binds to double-stranded DNA and emits the signal, co-relating with the amount of DNA of target sequence amplified.

The q-PCR procedure included 11 sets of primers that encode the PD-L1 (i.e. *CD274*) gene promoter region. In order to perform q-PCR, a diluted sample of cDNA was mixed with SYBR Green Master Mix (Bio-Rad), which contains dNTPs, a buffer solution, DNA polymerase, a

specific set of primers, and water. The mixture was then subjected to 40 cycles of incubation under the following conditions: an initial de-naturation step at 95°C for 10 minutes, followed by cyclicdenaturation at 95°C for 15 seconds, annealing of the primers at 60°C for 30 seconds, and the product extension: 72°C for 30 seconds. Moreover, it included a melting curve phase that included an increase in the temperature from 65°C to 95°C by 0.5°C after every 5 seconds.

The purpose of melting curve phase is to eradicate the false positive data.

The results of the reactions were carefully analyzed by using the 2^ (-ΔΔCT) method by following the strategies provided by Rao et al. (2013) in the publication.

Table 3.5: The ingredients and quantity for one PCR was utilized as mentioned below:

Reagents	Quantity
SYBR Green	5 µl
Primers	0.5 µl
DNA	2 µl
H2O	2.5 µl
Total Volume	10 µl

3.8: Isolation of RNA and Complementary DNA (cDNA) synthesis

Basically, reverse transcriptase enzyme transcribes mRNA to DNA sequence and that DNA is known as cDNA. It contains only exons which are the coding regions.

Total RNA isolation was performed using RNA isolation kit from Promega. For RNA isolation from cell lines, 1-5x10^6cells were used. Briefly, cells were suspended in BL buffer along with thioglycerol, 100%. After that isopropanol was added in order to precipitate the RNA, and then the mixture was applied to an RNA binding column and centrifugation was done at 12,000 rpm for 1 minute, at room temperature. The filtrate was removed and washed with a series of washing buffers included in the kit. RNA was eluted with RNase- and DNase-free water in a volume of 2530 µl.

The RNA is further subjected for the synthesis of complementary DNA (cDNA), using the Transcriptor First Strand cDNA Synthesis Kit (Roche Diagnostics) by following the

manufacturer guidelines. Initially, the template primer mixture was prepared that consisted of 1 µg of total RNA, 25µMAnchored oligo (dT) 18 primers (1 µl), 60 µM random hexamer primer (2 µl) in PCR grade water. It was centrifuged shortly and subjected to incubation in the thermal cycler for 10 min at 65°C in order to denature the RNA secondary structures, and then immediately placed on ice. Components of the RT mix that is comprised of Reverse Transcriptase Reaction Buffer, 5x concentrated (4 µl), Protector RNase Inhibitor40 U/µl (0.5 µl), Deoxy nucleotide, 1 mM each (2 µl) and Transcriptor Reverse Transcriptase, 20U/µl (0.5 µl) were added to this tube and centrifuged for a brief time. After that, the reverse transcription incubation reaction was performed in a thermocycler for 10min at 25°C, 55°C for 30 minutes, and then heated at 85°C for 5 min to inhibit the activity of reverse transcriptase. Complementary DNA was stored at -20°C for further experiments.

3.8.1: Real time Quantitative polymerase chain reaction (qRT-PCR)

The real time quantitative polymerase chain reaction (qRT-PCR) was conducted by using SYBR Green Master Mix (Bio-Rad), which contains dNTPs, a buffer solution, DNA polymerase, diluted cDNA, water and specific set of primers (for SWI/SNF subunits, EZH2 or PD-L1 gene). The PCR conditions included 40 cycles with an initial denaturation step at 95°C for 10 minutes, then cyclic denaturation at 95°C for 15 seconds, annealing of the primers at 60°C for 30 seconds, and extension of product, 72°C for 30 seconds. The ubiquitin was used as a control.

The results of the reactions were evaluated by using the 2^ (-ΔΔCT) method mentioned by Rao et al. (2013).

3.9: DNA Cloning

3.9.1: Amplification of the gene of interest

Polymerase chain reaction (PCR) was used to amplify the specific DNA sequence (i.e. coding PDL1) from L-1236 cell line from cDNA by following above mentioned protocol. Three different protocols were used for the multiplication of desired DNA sequence.

First polymerase chain reaction (PCR) was performed by using Sapphire mix, following the procedure provided by the manufacturer. The reaction involves the amplification of a selected DNA fragment (e.g. cDNA or plasmid), primers, deoxy ribonucleotides (dNTPs), polymerase

and water. The reactions were comprised of the following conditions: total number of cycles was 30.

1. Initial denaturation: 94°C for 1 minute.

   i. Cyclic denaturation: 98 °C for 5 sec. ii.
   Primer annealing: 54-64 °C for 5 sec.
   iii. Product extension: temperature depends on polymerase; time depends on the polymerase speed and product length (10 Sec/1Kb) i.e. 72 °C for 8 sec.

2. Final extension: 72 °C for 1min.

The correctness of the reaction was checked by horizontal gel electrophoresis in 1 % agarose gel.

Table 3.6: It demonstrates the quantity of reagents used for single reaction of thermo-cycler.

Reagents	Quantity
Sapphire Mix	5 µl
Primer Forward	0.2 µl
Primer Reverse	0.2 µl
DNA	0.5 µl
H_2O	4.1 µl
Total volume	10 µl

Another PCR reaction was conducted by using KAAPA mix, appropriate forward and reverse primers, cDNA and water as mentioned in Table 3.6. The PCR conditions were as mentioned below for both isoforms of PD-L1.

1. Initial denaturation 95 °C for 3 minutes.
2. Cycle repeated 30 times:
   i. Denaturation: 98 °C for 20 sec.
   ii. Attaching primers: 55 °C for 15 sec.
   iii. Product extension: 72 °C for 53 sec.
3. Final extension of the product: 72 °C for 3 minutes

Table 3.7: Quantity of reagents used to amplify the gene of interest i.e. PDL1.

Reagents	Quantity
Kappa Mix	5 µl
Primer Forward	0.75 µl
Primer Reverse	0.75 µl
cDNA	1 µl
H_2O	10 µl
Total volume	25 µl

The PCR conditions for amplification of FUS included as mentioned below:
1. Initial denaturation: 95 °C for 3 minutes.

i. Cyclic denaturation: 95 °C for 30 sec.
ii. Primer annealing: 56°C for 30 sec.
iii. Product extension: depends on polymerase, (Phusion enzyme) i.e. 72 °C for 2 minutes.

2. Final extension: 72 °C for 5 minutes. The number of cycles was 30.

The product was then purified by gel electrophoresis.

The amplified product was then checked by a horizontal gel electrophoresis.

Subsequently, the product was isolated from the gel and purified with an Agarose-Out kit. Alternatively, $1/10^{th}$ of PCR product was put on a gel (for verification of a successful amplification) and the remaining product was then purified using PCR product cleaning kit.

3.9.2: Agarose-Out DNA Purification

The Gene MATRIX Agarose-Out DNA Purification Kit is used for the isolation of ultra-pure linear and circular DNA molecules. It is applicable for the size ranging from 100 bp to 10 kb in size as well as TAE or TBE agarose gels. The kit was employed by considering the guidelines provided by the manufacturer.

In order to separate DNA, 30 µl of activation buffer was added to the spin column and left sit at room temperature until the mixture is transferred for the necessary membrane activation. After that, 2 volumes of orange-colored DX buffer were added for 1 volume of DNA so the total

volume of 40 µl. It was then applied to the DNA binding spin-column and centrifuged for one minute at 11,000 x g. Supernatant was discarded and the spin-column was placed in the receiver tube for a wash with 600 µl of Wash DX2 buffer. Spin column was put into a fresh receiver tube and the DNA was eluted by adding 50–150 µl of elution buffer and incubated for one minute at room temperature. Isolated purified DNA was stored at -20°C for further experiments.

3.9.3: PCR and DNA product purification

PCR and DNA Cleanup product kit DNA by Monarch® was used by adopting their provided protocol. The DNA sample was diluted with binding buffer with buffer to sample ratio 2:1 which is correct for dsDNA > 2 kb in size. The sample was loaded just after placing the column into the accumulating tube, centrifuged at maximum speed for 1 minute. The flow-through was then discarded and the column was reintroduced into collection tube and followed by washing with 200 µl of DNA Wash Buffer and again centrifuged at high speed for 1 minute. After that DNA was eluted by adding an elution buffer in a volume of 50 µl. It was incubated at RT for 1 minute and centrifuged for 1 minute.

3.9.4: DNA Digestion

Another crucial step in cloning is the digestion that involves the use of restriction enzymes. Both amplified gene of interest and cloning vector (pGAD424, pGBT9) were digested by the appropriate restriction enzyme pair to produce same ends. For digestion of the PD-L1 the restriction enzymes were *Eco*RI and *Sal* I and for the FUS – *Bam*HI and *Sal* I).

The important fact is that the inserts contained sequences recognized by the appropriate restriction enzymes at ends added by the primers during the PCR reaction.

Table 3.8: It displays the amounts of reagents that were used to the restriction digestion reaction.

Reagent	Quantity
10x Fast Digest™ buffer	1 µl
Enzyme I	0.5 µl
Enzyme II (optional)	0.5 µl
Insert/plasmid	1-3 µl
H_2O up to total volume	10 µl

The reaction mixture as mentioned above was conducted by keeping it for incubation 15-30 minutes at 37 °C. The cleaved product was then subjected for horizontal electrophoresis in 1% agarose gel. The pattern of bands corresponding to the cleaved fragments and plasmid ensured the correctness of digestion, without using Sanger sequencing. After that DNA with appropriate size was cut down from the agarose gel using a sterile scalpel. That was further subjected for cleaning and purification from the gel by the Agarose Out kit (EurX) by pursuing the instructions of manufacturer as mentioned above.

3.9.4.1: Verification by horizontal gel electrophoresis

The agarose gel was prepared by weighting the proper quantity of the dry agarose and dissolving in 1x TBE buffer along with ethidium bromide. The solution was then heated and cooled down, then poured into caster with a multi-hole comb and allowed to set completely. Restriction digest products were then loaded into wells. After that horizontal electrophoresis was performed at a voltage of 75-90 Volts, for 30-40 minutes depending on the fragment size. A trans-illuminator was used to visualize the DNA/RNA at a wavelength of 302 nm.

3.9.5: Ligation

The digested product i.e., vector and gene of interest, were ligated by using DNA ligase in order to covalently join the ends of the vector and the coding sequence in the insert. This resulted in recombinant DNA molecules. The ligation reaction was settled down in a tube having the ingredients in the following quantity as mentioned in Table 3.9.

Table 3. 9: It shows the amounts of reagents that were used to carry out the ligation reaction.

Reagent	Quantity
Digested/cleaved PCR product (FUS, PD-L1)	Up to 17 µl
Buffer	2.5 µl
Plasmid (PGAD424/PGBT9)	1 µl
Ligase Enzyme	1 µl
H_2O	x µl
Total volume	25 µl

The ligation reaction was performed at 16°C overnight. Ligase activity was inhibited by incubation at 65°C for 10 min.

3.9.6: Bacterial transformation by the heat shock method

The recombinant plasmid DNA was introduced into bacteria *Escherichia coli* DH5α. The procedure included thawing on ice of one tube of previously prepared heat-shock competent bacteria on ice for 10-15 minutes. The appropriate amount (usually up to 10 µl) of ligated plasmid mixtures (PGAD424 or PGBT9), after the ligation reaction were added to *Escherichia coli* DH5α was and were incubated on ice for 30 minutes. Subsequently, the tube with the mixture was transferred to 42°C for 1 minute and then immediately transferred back to ice and kept for 5 minutes. 900 µl of fresh liquid broth without antibiotics was added and mixed well. It was incubated for 1 h at 37°Cwith shaking 190-220 rpm. Then the mixture was centrifuged at 12,000 rpm, for 1 minute at RT, excess supernatant was poured off. The pellet was resuspended in 200-250 µl medium and poured onto LB agar plates that had a selective antibiotic (carbenicillin) for screening of transformed cells. The plates were incubated at 37°C overnight. So, those cells that gained the vector (with the gene of interest) survived successfully on plates.

3.9.7: Verification of transformation

There are different methods used in order to verify the presence of gene of interest in the colonies of transformed cells, including PCR and DNA sequencing or restriction mapping following the plasmid DNA isolation. In this work the plasmid isolation and analysis were used preferentially.

3.9.8: Plasmid Isolation

Plasmid isolation was done by following different protocols that included mini preps and maxi preps by following protocols.

Plasmid DNA was isolated from transformed bacteria after overnight culture (12-16 hours after inoculation) with the carbenicillin antibiotic using the Plasmid Mini-prep System and QIAGEN® Endo Free Plasmid Maxi Kit according to the protocols provided by the manufacturers.

i. Plasmid Mini-prep System

The cultures after the overnight incubation were centrifuged 16,000 x g for 5-7 minutes and pellet was resuspended in buffer B1 and vortexed well. After that, lysis Buffer B2 was added and mixed by inverting several times. Then neutralizing buffer B3 was added, and samples were centrifuged to pellet the neutralized cellular debris. After that, the supernatant was applied to appropriate columns and centrifuged. Plasmid DNA attached to the column bed was washed several times with the provided washing buffers. Then, the plasmid DNA was eluted with DNase and RNase free water or the provided elution buffer. After isolation, the concentration of the obtained DNA plasmid was measured spectro-photometrically by the Nanodrop™ 2000 device.

ii. QIAGEN® Endo Free Plasmid Maxi Kit

In short, the overnight bacterial culture was harvested by centrifugation at 4°C for 15 minutes, resuspended in P1 buffer and then P2 buffer was added, sample was mixed thoroughly at room temperature and kept for 5 minutes. Then the chilled P3 buffer was added, and the entire mixture was mixed well but gently. This lysate was then poured into the QIA filter Cartridge barrels and incubated for 10 minutes, then filtered. After that ER buffer was added and it was incubated for half an hour on ice. It was further followed by adding QBT buffer to equilibrate the QIAGEN-tip column and the lysate was passed through the column. The QIAGEN-tip was washed by QC buffer three times. DNA was then eluted by QN buffer and precipitated by isopropanol at room temperature. The mixture was centrifuged 15,000 x g at 4°C for 30 minutes. Then the supernatant was discarded and washed with 70% ethanol. The pellet was then air dried and re-suspended in TE buffer.

iii. Colony PCR

Colony PCR was also used to confirm the transformation of desired gene into a vector. After the transformation, colonies from plates were picked and suspended in 10 µl of sterile injection water and put at room temperature for 10 minutes. Then it was kept first for 20 minutes at -80 °C and then at 95 °C for 10 minutes. Subsequently it was subjected to the PCR by following conditions.

The total number of cycles was 30.

1. Initial denaturation: 94°C for 1 minute.

i. Cyclic denaturation: 98 °C for 5 sec.

ii. Primer annealing: 55 °C for 5 sec.

iii, Product extension: temperature depends on polymerase; time depends on the polymerase speed and the product length.

2. Final extension: 72 °C for 5min.

The composition of the reaction mixture is given in the table below (3.10).

After verification of PCR product on 1% TBE gel, the plasmid DNA was isolated from the positive clones and then it was sent for sequencing.

Table 3.10: Amounts of reagents used for single thermo-cyclic reaction.

Reagent	Quantity
DNA	10 µl
10x Fast buffer	2 µl
Forward primer	1 µl
Reverse primer	1 µl
dNTPS	1 µl
Taq polymerase	0.3 µl
MgCl2	0.5 µl
H_2O	4.2 µl
Total volume	20 µl

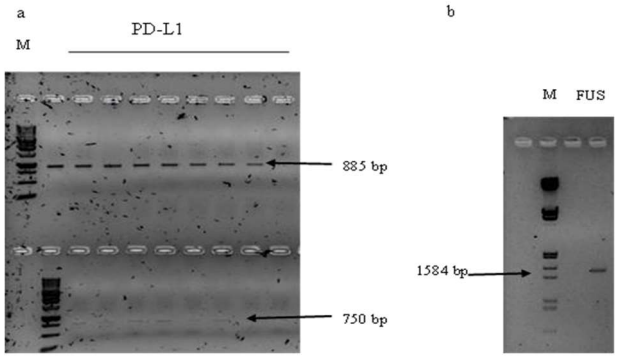

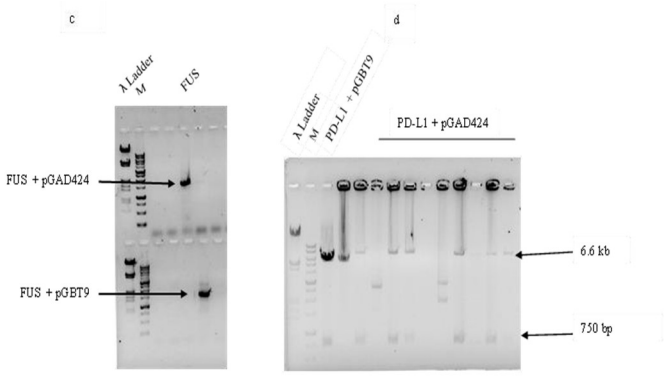

Figure 3.1: Cloning strategy for PD-L1 and FUS protein.

Image (a) and (b) depict the PCR product of gene of interest i.e., PD-L1 (Isoform 1 and 4) and FUS after amplification with their respective product size. Image (c) represents the positive insertion of FUS coding sequence into plasmids pGAD424 and pGBT9, respectively alongwith λ DNA *Eco*RI/*Hin*d III digest (molecular size marker), while image (d) shows the confirmation of effective insertion of PD-L1 (isoform 4) coding sequence into pGBT9 and pGAD424 plasmids. After digestion with restriction enzymes *Eco*RI and *Sal*I the respective plasmids and their inserts are visible.

The constructed plasmids pGBT9 and pGAD424 with the genes of interest which are PD-L1 isoform I, PDL1 isoform IV and FUS (RNA binding protein) coding sequences are shown in Figure 4.13. Their sequences are in agreement with the model that was created *in silico* by ApE- A plasmid Editor (v3.08) software and were confirmed by Sanger method sequencing.

Figure 3.2: Plasmid maps of pGBT9 and pGAD424 for PD-L1 isoform I, PD-L1 isoform IV and FUS.

Image (a) represents cloned PD-L1 isoform I in pGBT9 and pGAD424, image (b) depicts the PDL1 isoform IV cloning in pGBT9 and pGAD424, and image (c) shows FUS cloning inpGBT9 and pGAD424 plasmid respectively, genes responsible for the selection and Gal4 domains are also mentioned. Moreover, other candidate proteins believed to interact with PD-L1, including BAFF 155, AMPK, SLUG, and SNAIL, were also previously cloned into pGBT9 and pGAD424 plasmids. These candidate proteins were identified as potential interactors and the cloned sequences coding them were obtained from the Department of ZIE. Plasmids pGAD424 and pGBT9, which contain different candidate proteins (BAF155, SNAIL, SLUG, AMPK and FUS), were used in combinations with the appropriate plasmids coding PD-L1 isoforms I and IV to further confirm the potential interactions by using yeast two-hybrid system (Figure 4.14).

3.9.9: Preparation of stocks of transformed cells for future experiments

Bacteria carrying appropriate plasmids were stored as stocks in LB medium containing 20-25% glycerol. They were kept frozen at -70°C.

3.10: Yeast two hybrid system (Y2HS)

The Y2H assay is based on a reporter gene expression. It is activated by a transcription factor having DNA-binding domain (BD) and an activation domain (AD). The protein termed as bait is fused with the BD, the other one, called pray, is attached to the AD. The physical proximity of the two proteins of interest brings AD and BD domains together, reconstituting the transcription factor activity and thus activating the expression of the lacZ reporter gene what results in the production of β-galactosidase. The consequence is the blue pigmentation, showing successful interaction between proteins.

3.10.1: Yeast cultivation

Yeast was grown on 10 cm diameter petri plates on YPD medium at 30°C for 2– 3 days.

3.10.2: Yeast transformation

The process of transformation is termed as one step transformation and it was done by adding 5 µl of carrier DNA (DNA from salmon sperm) to 100 µl of yeast transformation buffer, appropriate amount of plasmid DNA that was usually 2-5µl then added into a tube that had a loop full of Y190 yeast culture. The yeast was collected from the plate with a sterile loop and

suspended in the tube with DNA. The mixture was vortexed and mixed well and then incubated at 45°C for 30 minutes. After that the mixture was plated onto petri plates with the appropriate selective media and was incubated for 3-4 days at 30°C.

3.10.3: X-gal based screening technique

X-gal or blue-white colony screening test was performed to verify the protein-protein interaction. In this technique, the functional LacZ gene that encodes ß-galactosidase causes the blue pigment to appear in the presence of X-gal.

The successfully transformed colonies of Y190 yeast strain were sub-cultured on selective media plates i.e., SD-leu -trp dishes (without leucine and tryptophan), SD-leu dishes (without leucine) and SD-trp dishes (without tryptophan) for 2-3 days and subjected to transfer on disc or round shape Hybond N+, respectively. This membrane with yeast colonies was kept in liquid nitrogen for 15-20 seconds and put on the 10 cm dishes containing disks or round shape of chromatography paper, soaked with 3 ml Z-buffer with β-mercaptoethanol (10 µl) and X-gal (80µl). The plates were incubated for 1 hour at 37°C. The PCL-1 was used as positive control. The appearance of blue pigmentation referred to positive and white as the lack of interaction between proteins. The intensity of blue color shows the intensity of interaction.

3.11: Flow-cytometry

After growth of cells and their collection, 1 million cells were suspended in 100µl PBS buffer with

1%FBS at 4°C in the dark. Subsequently, antibodies like anti-CD3: 5 µl, anti-CD279-PE, antiCD273-APC, anti-CD274-PE (10 µl) were added to the respectively labeled tubes. They were vortexed and incubated at 4ºC for 25 minutes. Again, 1.8 ml PBS/1%FBS was added to the each FACS-tube and centrifuged at 400xg for 10 minutes. The supernatant was discarded from each tube and cells were re-suspended in 100µl PBS/1%FBS buffer at 4°C. Then 6 µl 7-AAD were added, and tubes were incubated at 4°C for 10 minutes in the dark. Once more 0.4 ml PBS/1%FBS was added, and the tubes were subjected to vortex. After this labeling, analysis was performed by BD FACS ARIAIII.

Table 3.11: The pattern and combination of fluro-chrome used for labelling of CD279 (PD-1), CD274 (PD-L1), CD273 (PD-L2), 7-AAD and CD3, while autofl depicts the absence of any applied labels.

Reaction (tube) number	FL 1	FL 2	FL 3
1	autofl.	autofl.	autofl.
2	autofl.	**7-AAD**	autofl.
3	**CD279 (PD-1)-PE**	**7-AAD**	autofl.
4	**CD274 (PD-L1)-PE**	**7-AAD**	autofl.
5	autofl.	**7-AAD**	**CD273 (PD-L2)-APC**
6	autofl.	**7-AAD**	**CD3-APC**
7	**CD3-PE**	**7-AAD**	autofl.
8	**CD279 (PD-1)-PE**	**7-AAD**	**CD273 (PD-L2)-APC**
9	**CD274 (PD-L1)-PE**	**7-AAD**	**CD273 (PD-L2)-APC**
10	**CD274 (PD-L1) -PE**	**7-AAD**	**CD3-APC**
11	**CD3-PE**	**7-AAD**	**CD273 (PD-L2)-APC**

3.12: MTT Assay

Selected cell line was seeded in 96-well plates in the number of 100000 cells per well.

All cells were seeded in triplicate for each experimental condition. The EZH2 inhibitor i.e. Tazemetostat (EPZ-6438) was added to the growing cells as 5-fold serial dilution (concentrationswere 0.052, 0.26, 1.3, 6.5, 32.5 µM, volume was 1.3 µl) and 2 µl of1% DMSO as the untreated control. Plates were incubated for 3 days at 37°C, 5% CO_2 and 100% humidity. After 72 hours from seeding, thiazolyl blue tetrazolium bromide (MTT solution; 5g/ml in PBS)

was added to the cells to obtain 10% solution in the medium. The cells were then incubated for 3 h at 37°C, 5% CO2 and 100% humidity, allowing formazan crystals to form. Then the plate was centrifuged for 3 minutes at 350 RCF at 4 °C. MTT medium was removed and 50 µl of pure DMSO was added to the wells. In order to dissolve the formazan crystals; it was incubated for 1 h on a rotator in darkness. The signal was then measured spectrophotometrically at a wavelength of 540 nm. For each condition, the experiment was performed in at least three repetitions. The obtained results were presented in the form of curves showing viability rates and IC50 values were determined for tested cell line against EPZ-6438 inhibitor.

Cell lines treated with inhibitor along with negative control and DMSO were then subjected for western blot analysis to further confirm the results and influence of this epi drug against PD-L1, BRM, BAFF 155, PD-L2, Methylated Histone and Histone protein level.

4. RESULTS

4.1: The evaluation of cHL cell lines from NIO repository

In order to gain comprehensive understanding of PD-L1 function not only outside of the cell on the cell surface but also inside of the cell, the human cell line models of Classical Hodgkin Lymphoma were used: KM-H2, L-1236 and L-428. cHL has characteristic hallmarks; therefore I performed further analysis to select proper cell line for further experiments. At first, all the cells were authenticated by the external licensed service (CeGaT GmbH, Germany).

4.1.1: Observation of cells of classical Hodgkin Lymphoma cell line using light microscopy

The lymphoma cells are growing in suspension and growth pattern depends on cells density, therefore I frowth all cHL cell lines and evaluate them under light microscope.

Figure 4.1: Visualization of cells after growth under light microscope.

The cells of classical Hodgkin Lymphoma were visualized under light microscope to check their viability and growth pattern (Figure 4.1). The cells after growth were collected and stored at 80°C to conduct further experiments.

4.1.2: Nuclear pattern analysis of HRS cells by confocal microscopy

HRS cells are characterized as multinucleated cells; therefore confocal microscopy was used to confirm that all lines are cHL cell lines. The double and multiple nuclei of Hodgkin cells is one

of the key hallmarks of cHL. Among all analyzed cell lines, in L-1236 cHL cell line, all types of nuclei were observed (single, double, and multi-nuclei) notably (Figure 4.2).

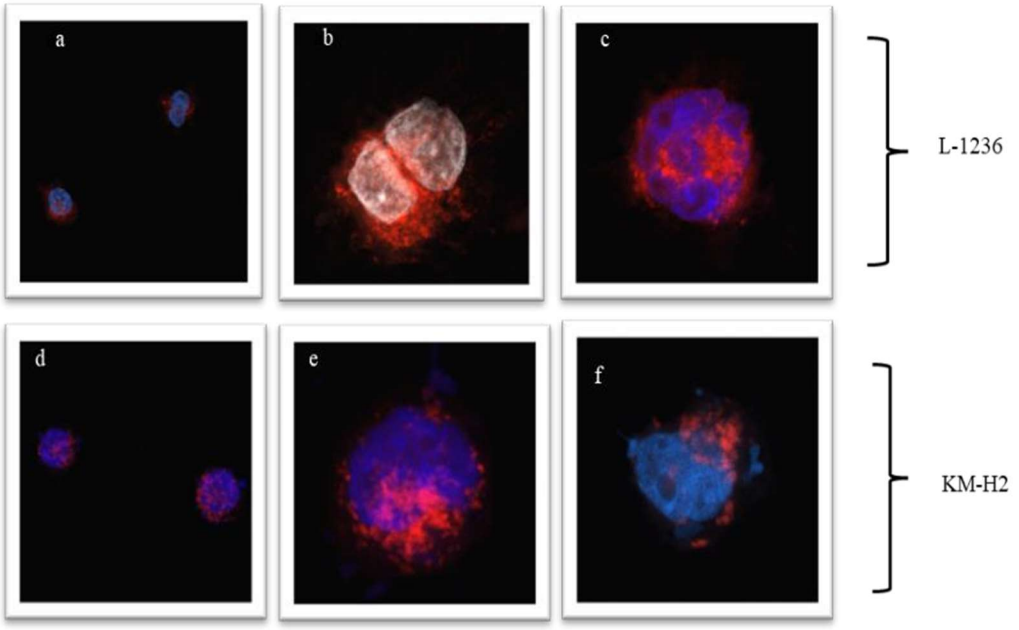

Figure 4.2: Confocal microscopy of KM-H2 and L-1236 cells depicting the typical nuclear patterns for HRS cells.

The cells from cell lines of Hodgkin disease exhibit nuclear heterogeneity. Some of the images (a, d, and e) represent the uni-nuclear Hodgkin cells while others (b, f, and c) show the presence of Reed-Sternberg cells with two or more nuclei, respectively. Moreover, the red color represents the mitochondria of cells (with detection wavelength 574-700 nm), and blue color depicts the cellular nuclei (DAPI staining with detection wavelength 400-490 nm).

4.1.3: CD-30 protein expression detection in cHL cell lines

One of the hallmarks of cHL is overexpression of CD30 on HRS cell surface; therefore I performed Western blot analysis. Initially the lysates from all cell lines were analyzed by SDS PAGE and transferred onto a PVDF membrane for Western blotting (Figure 4.3). That was further subjected to check the expression of CD30 protein. For loading control I used gel containing 0.5% TCE and proteins were visualized using UV light.

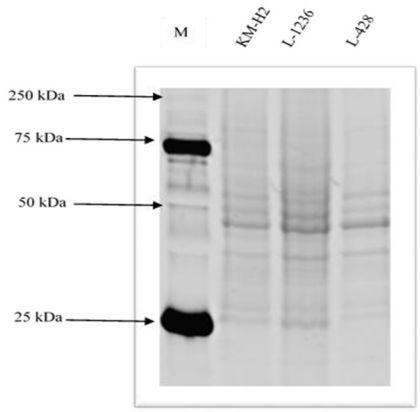

Figure 4.3: Visualization of proteins by TCE from cHL cells (KM-H2; L-1236 and L-428) along standard protein size marker (M).

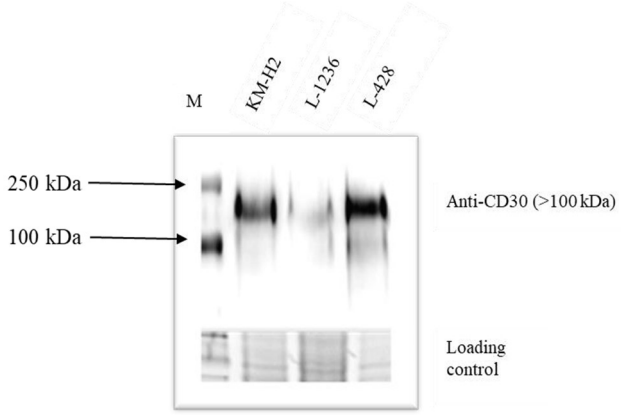

Figure 4.4: Expression of cHL marker CD30 in three used cell lines. As loading control, the stain free (TCE) method was used.

The expression of CD30, a key marker of cHL was observed in all examined cell lines (KM-H2, L-1236 and L-428) (Figure 4.4). It further gives authentication of cell lines from classical Hodgkin lymphoma.

4.1.4: Assessment of the expression of PD-L1 in cHL cell lines

All of these experiments confirmed that all examined cHL cell lines obtained from MSCNRIO biobank repository were Hodgkin lymphoma HRS cells. After confirming cHL identity, Western blotting and qRT-PCR was used to assess PD-L1 expression in cHL cell lines.

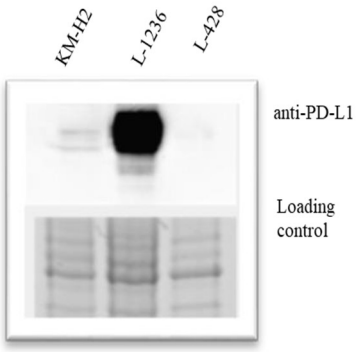

Figure 4.5: PD-L1 is highly overexpressed in L-1236 HL cell line comparing to KM-H2 and L-428. As a loading control the stain free method was used (based on TCE fluorescence).

The analysis of PD-L1 expression by western blotting revealed that the strongest PD-L1 overexpression is present in L-1236 cell line as compared to other cell lines (Figure 4.5). Moreover it was further confirmed by performing qRT-PCR.

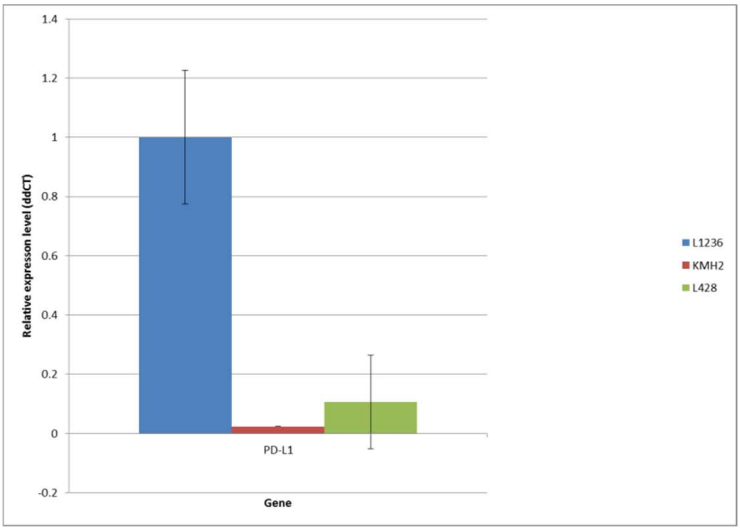

Figure 4.6: Analysis of PD-L1 expression by qRT-PCR in all cHL cell lines

The qRTPCR showed that the gene encoding PD-L1, depicted high level of expression in L-1236 cell line as compared to other mentioned cell lines (Figure 4.6). That is in line to the results of overexpression of PD-L1 protein from western blot study. Basically, L-1236 depicted the high level of expression, KM-H2 average level of expression, while L-428 almost the lowest level of PD-L1 expression.

Overexpression of PD-L1, CD-30 expression and the presence of bi- and multi-nuclear pattern in L-1236 cell line sparks great interest and curiosity and that is why this cell line has been selected for further experiments.

4.1.5: Detection of PD- L1 expression on cell surface of L-1236 HL cell line

The PD-L1, as previous data suggest, is a transmembrane protein and usually expressed on cell surface. PD-L1 on the cell surface bond with its counterpart receptor PD-1 on T cell surface and modulate the T cell activity and immune responses. Therefor we use the flow cytometry to analyze the abundant of PD-L1, PF-L1 and PD-1 protein on the cell surface. In these assays cells from L1236 cell line were labeled with fluorescently conjugated antibodies that target PD-L1, PD-L2 and PD-1 (Figures 4.7 and 4.8) to check their cellular localization, their expression at the single-cell level and quantitative information about cells expressing this protein.

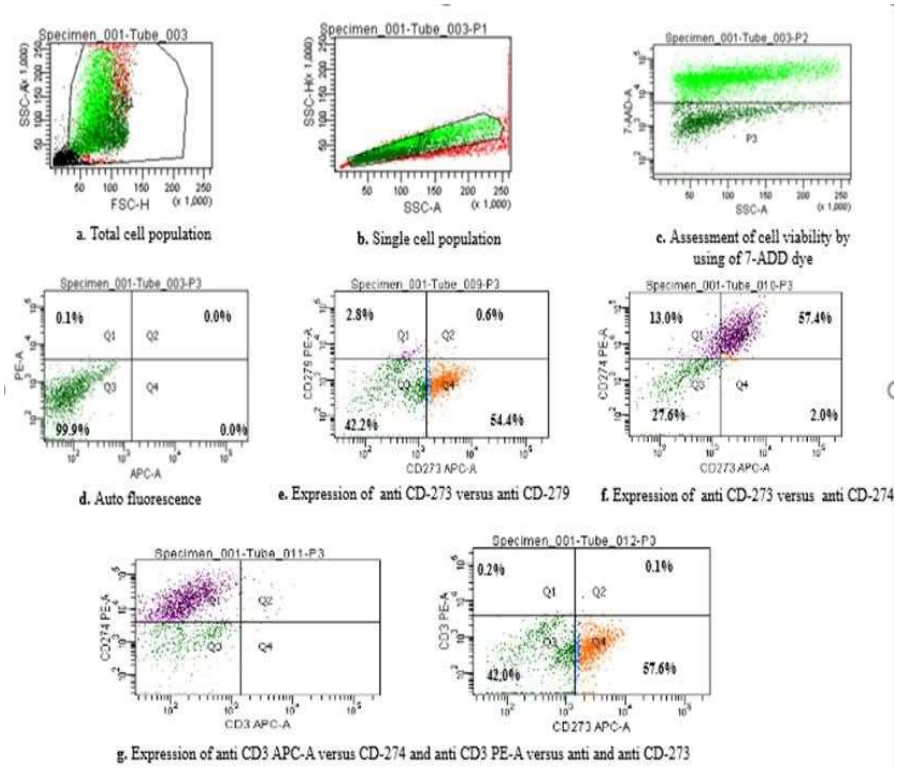

Figure 4.7: Dot plots showing the analysis of expression of CD-273, CD-274 and CD-279 on the surface of L-1236 Hodgkin cell lines.

The data from flow cytometry confirmed the expression of CD274/PD-L1 (70.4%) and CD273/PD-L2 (59.4%) while CD-279/PD-1 was considered to have no or extremely low expression on the cell surface. Moreover, samples labeled with anti CD3 monoclonal antibody were used as a negative control for unspecific binding.

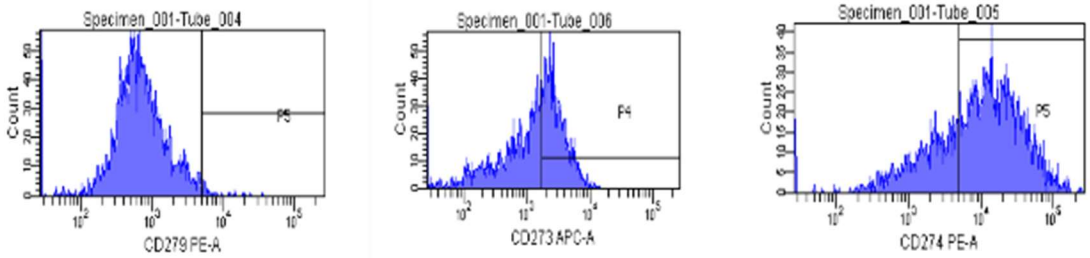

Figure 4.8: Histogram showing the analysis of samples labeled with anti CD273, anti CD274 and anti CD279 monoclonal antibodies on the surface of L-1236 cell line.

4.2: Assessment of the expression of SWI/SNF complex and PRC2EZH2 subunit expression in cHL cell lines

Considering the fact that SWI/SNF complex and Polycomb Repressive Complex 2 (PRC2) participate in PD-L1 expression at chromatin level in T cells (Jancewicz et. al. 2021), the protein level of SWI/SNF subunits (BRM, INI1) and EZH2 – a PRC2 subunit in all cHL cell lines has been analyzed (Figure 4.9).

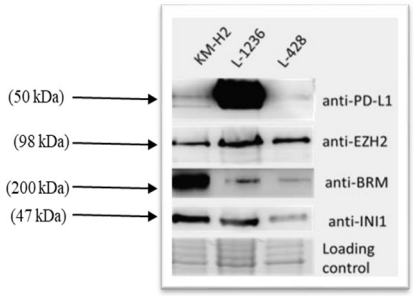

Figure 4.9: Western blot analysis of expression of SWI/SNF subunits BRM, INI1 and EZH2 a Polycomb Repressive Complex 2 subunit in all three cHL cell lines. As a loading control, a stain free (TCE) method was used.

Most interestingly, in L-1236 line (with PD-L1 overexpression) the low amount of SWI/SNF subunits BRM and INI1 was observed what parallels high expression of EZH2. On the other hand, KM-H2 cell line showed low level of expression of PD-L1 and elevated expression of BRM which is followed by INI1 and EZH2, respectively. In contrast, SWI/SNF subunits (INI1 and BRM) depicted lower level in the L-428 cell line that also exhibits lower expression of PD-L1protein.

Furthermore, to assess the relation between the protein and transcript levels expression of examined proteins (PD-L1, BRM, and EZH2), the qRT-PCR was performed (Figure 4.10).

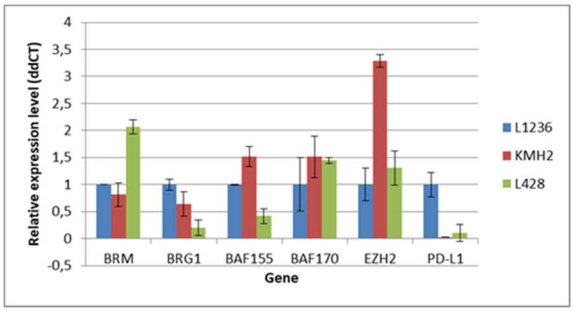

Figure 4.10: Expression level of genes encoding for SWI/SNF subunits, EZH2 and PD-L1 proteins in all three cHL cell lines. As a reference the ubiquitin gene was used.

The transcript levels of SWI/SNF subunits and EZH2 differ between the cell lines and differ from protein level. This results may indicate another mechanism of protein amount regulation not only transcript level.

4.3: Subcellular localization of PD-L1

The main function of PD-L1 is related to the surface PD-L1, but in cHL the revers signaling of PD-L1 was described as well as PD-L1 may exist in soluble fraction, therefore I checked the exact cellular localization of PD-L1 in HRS cells. The isolation of cytoplasm and nuclei was performed for the L-1236 cell line. The Western blot analysis was further performed using anti–PD-L1 specific antibody. The result showed the presence of PD-L1 not only on the cell membrane of HRS cells but also in the nucleus. As a nuclear fraction marker, the histone H3 was used (Figure 4.11)

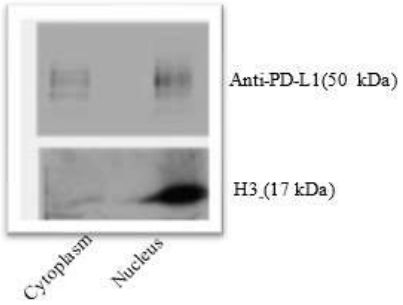

Figure 4.11: Subcellular localization of PD-L1 in L-1236 (cHL) cell line.

The presence of PD-L1 in the cell nuclei may indicate their different, not ligand for PD-1, function.

4.4: Identification of nuclear PD-L1 binding partners

The PD-L1 was observed in the cell nuclei in HRS cells, therefore it has been decided to evaluate the exact role of nuclear PD-L1 in these cells as well as to find potential nuclear partners of PDL1. The immunoprecipitation (IP) method with anti-PD-L1 antibody on the lysate from isolated cell nuclei of L-1236 cell line was performed (Figure 4.12), followed by mass spectrometry analysis. The experiment was performed three times and samples were sent for mass spectrometry analysis to the Institute of Biochemistry and Biophysics in Warsaw. The obtained results were further analyzed and proteins which were present in high score in at least two replicates and not present in IgG control samples were considered as potential nuclear PD-L1 partners and their potential function were also predicted (Table 4.1).

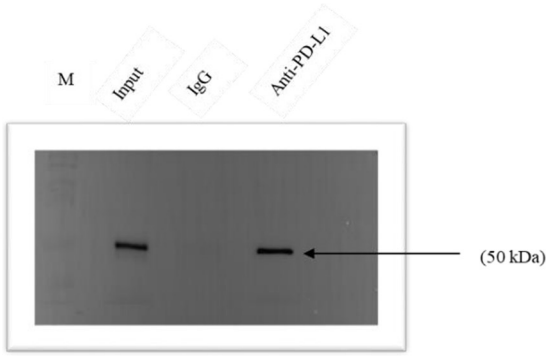

Figure 4.12: Immunoprecipitation of PD-L1 in L-1236 (cHL) cell line.

Immunoprecipitation of nuclear PD-L1 was done for the detection of nuclear interacting partners of PDL1. The presence of PD-L1 in particular samples using Western blot was confirmed. IgG was used as a control.

Table 4.1: Potential nuclear partners of PD-L1 and their functions after immunoprecipitation and mass spectrometry analysis.

Mass spectrometry results for potential interactors of PD-L1		Functions
1	RNA-binding protein FUS	RNA binding; transcription co-regulator activity; mRNA stabilization; regulation of RNA splicing; regulation of gene expression; maintenance of genomic integrity
2	Splicing factor 3B subunit 1	mRNA binding; splicing factor binding; positive regulation of transcription by RNA polymerase III, mRNA splicing, via spliceosome
3	Serine/arginine-rich splicing	mRNA processing; regulation of alternative mRNA

	factor 2	splicing, via spliceosome
5	Small nuclear ribonucleoprotein Sm D2	RNA splicing, spliceosome complex assembly
6	Transformer-2 protein homolog beta	mRNA binding; protein domain specific binding; mRNA splicing
8	Heterogeneous nuclear ribonucleoprotein U	mRNA processing; RNA splicing
9	Y-box-binding protein 1	Regulation of transcription and translation; pre-mRNA splicing; DNA reparation; mRNA packaging
10	RNA-binding protein with serinerich domain 1	mRNA splicing, via spliceosome and regulation of alternative mRNA splicing; positive regulation of apoptotic process
11	Splicing factor U2AF 65 kDa subunit	Enzyme binding; pre-mRNA 3'-splice site binding; mRNA splicing RNA binding, mRNA processing; negative regulation of protein ubiquitination
12	Serine/arginine-rich splicing factor 11	Pre-mRNA processing, alternative splicing

Surpristingly, mass spectrometry analysis reveald that nuclear PD-L1 may be involved with interaction with RNA processing proteins.

4.4.1: Nuclear PD-L1 interacts with SWI/SNIF complex and EZH2 subunit

In addition to the exploration of the role of nuclear PD-L1 in RNA processing, particularly in splicing, its interaction with other proteins like EZH2- a PRC2 complex subunit and SWI/SNF subunits (BRM, BAF155 and INI1) (Figure 4.13) have been also investigated through directional immunoprecipitation, suggesting potential regulation of gene expression at the chromatin level.

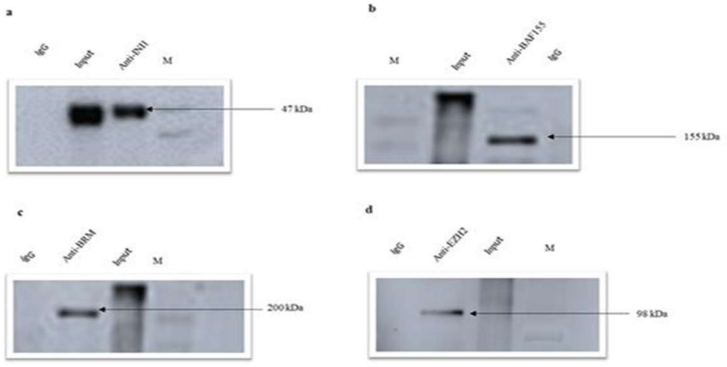

Figure 4.13: Co-immunoprecipitation of SWI/SNF subunits and EZH2- a PRC2 complex subunit from L-1236 Hodgkin cell line with PD-L1. The image depicts the results of the Western Blot for (a) INI1, (b) BAF155, (c) BRM and (d) EZH2 proteins, respectively, along with their inputs and IgG as a control.

The results indicated the potential role of nuclear PD-L1 not only on the RNA processing but on the chromatin level.

4.5: Chromatin immunoprecipitation (ChIP)

After immunoprecipitation, to confirm the presence of potential nuclear partners of PD-L1 and their function in the regulation of gene expression at chromatin level at the promoter region of PDL1, chromatin immunoprecipitation was performed, followed by qPCR. Chromatin-IP assays confirmed the binding and presence of PD-L1 protein itself, SWI/SNF subunits (BAF 155), and EZH2 (PRC2) at *CD274* (*PD-L1*) promoter in HRS cells along with methylated and acetylated Histone H3 (Lys27). The analyzed data by following 2ˆ(-delta delta CT) method (from Rao et al., 2013), revealed that BAF155 and EZH2 are found at the same regions as acetylated histone H3 and methylated histone H3 (Figure 4.14 a).

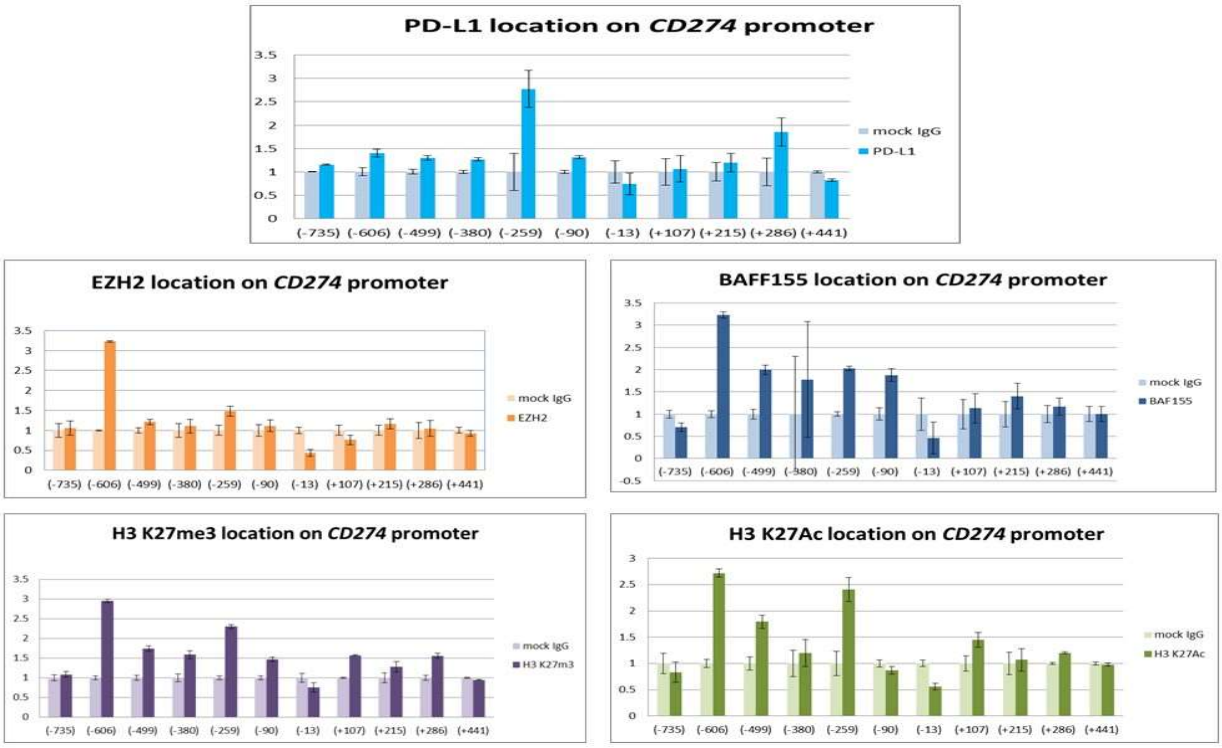

Figure 4.14 a: Analysis of q-PCR data after Chromatin Immunoprecipitation (ChIP) of *CD274* promoter region for location of subunits of SWI/SNF (BAFF 155), PCR2 complex (EZH2), PD-L1, methylated histone H3 and acetylated histone H3.

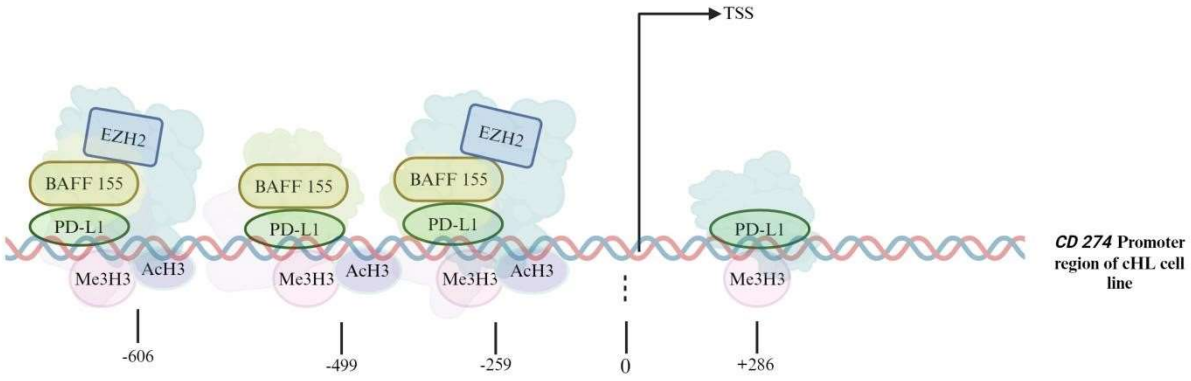

Figure 4.14 b: A systematic model representing the protein binding pattern on the PD-L1 locus of cHL cell line.

PD-L1 loci show the presence of both methylation and acetylation of histone H3K27, PD-L1, BAFF155 and EZH2 binding at the positions (-606 and- 259) while BAFF155 and PD-L1 located at the position (-499) along with methylated and acetylated histone, and PD-L1 with methylated histone at the position (+286).

These results suggest the regulation of CD274 expression via interplay of SWI/SNF and PRC2 complexes together with nuclear PD-L1.

4.6: Detection of protein-protein interaction by Yeast two-hybrid system

After detection of potential nuclear binding partners of PD-L1 by co-immunoprecipitation assay, SWI/SNIF complex and EZH2 subunit considered to be nuclear partner of PD-L1. In addition, the results from mass spectrometry, FUS RNA binding protein was found to be one of the potential partner especially with the components of the splicing machinery as mentioned in Table: 4.1. So, to further confirm the possible interactions of PD-L1 protein, suggested by the mass spectrometry results, the yeast two-hybrid system has been used, that actually detects the protein-protein interactions *in vitro*. Thus, the sequences encoding PD-L1 isoform 1 and isoform 4, along with FUS were amplified and cloned into plasmids pGBT9 and pGAD424, components of the yeast system for the confirmation of interaction.

Moreover, other candidate proteins were believed to interact with PD-L1, including BAF155, AMPK, SLUG, and SNAIL. These candidate proteins were identified as potential interactors and

the sequences coding them (obtained from the Department of Experimental Immunotherapy) were cloned into pGBT9 and pGAD424 plasmids. Plasmids pGAD424 and pGBT9, which contain different candidate proteins (BAF155, SNAIL, SLUG, AMPK and FUS), were used in combinations with the appropriate plasmids coding PD-L1 isoforms 1and 4 to further confirm the potential interactions by using yeast two-hybrid system (Figure 4.15).

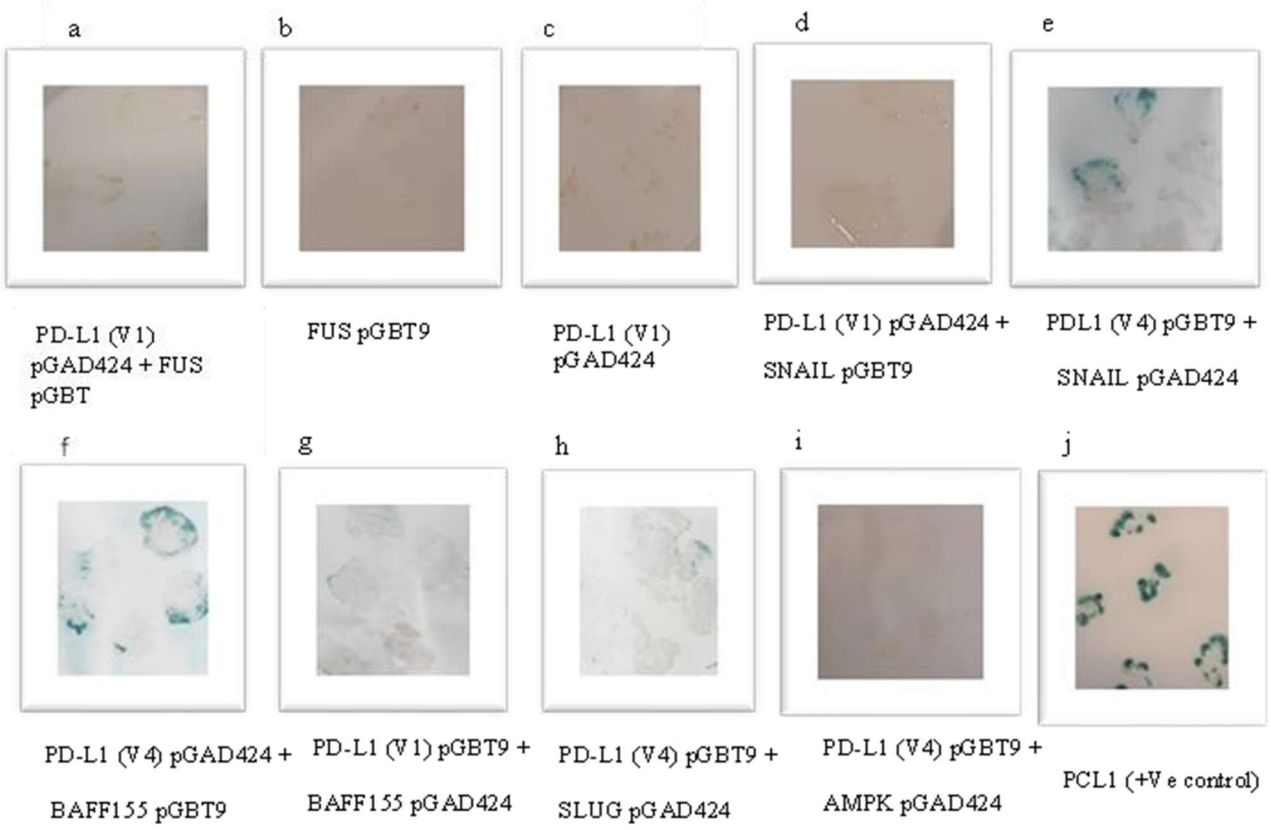

Figure 4.15: Analysis of protein-protein interactions using Y2H assay.

Blue colonies and greenish blue ones indicate the interactions of protein PD-L1 isoform 1 and 4 with potential interactor proteins i.e., FUS, SNAIL, BAF155 and SLUG (represented in image a, e, f, g, and h) respectively. Image (j) denotes the positive control, while no interaction was observed for AMPK (i). Particularly, for previously examined (co-immunoprecipitation on L-1236 line) proteins FUS and BAFF155 using the yeast system allowed us to re-confirm the interactions. Additionally, interactions between PD-L1 and SNAIL, SLUG, apart from the protein AMPK were observed.

4.7: Detection of EPZ-6438 inhibitor effect on cells by MTT Assay

Tazemetostat (also known as EPZ-6438) was used as an EZH2 inhibitor. Its function is to block the catalytic activity of EZH2, thereby inhibiting the methylation of histone H3 at lysine 27 (H3K27me3). This inhibition leads to alterations in expression of genes, affects cell proliferation, differentiation, as well as survival. The MTT assay was done to check the cell viability after the treatment of cells of L-1236 cell line with this epi-drug and to assess its effect on PD-L1 expression. For this purpose, the effective concentration of this compound was determined by using the series of dilutions (0.052, 0.26, 1.3, 6.5, 32.5 µM) for 48 hours.

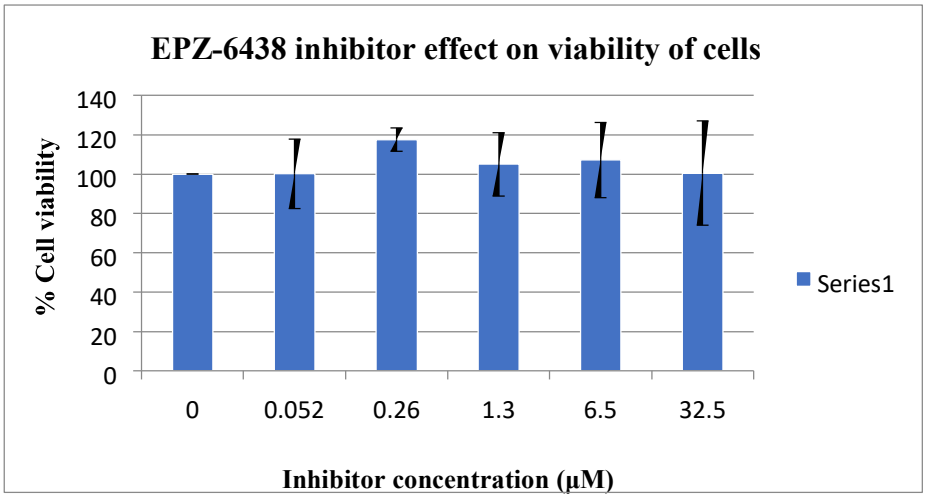

Figure 4.16: The effect of EPZ-6438 inhibitor on L-1236 cHL cell line.

There are different concentrations of EZH2 inhibitor that were applied to check their impact on the growth and survival of the cells from L-1236 cell line. No reduction has been recorded in the cell survival in the MTT assay after 48h.

4.7.1: Impact of EPZ-6438 inhibitor on levels of target proteins by Western blot analysis

L-1236 cells after treatment with EPZ-6438 inhibitor at the previously established concentration were checked by Western blot analysis. The negative control was individual cell cultures treated with DMSO or cells without any treatment (Figure 4.17).

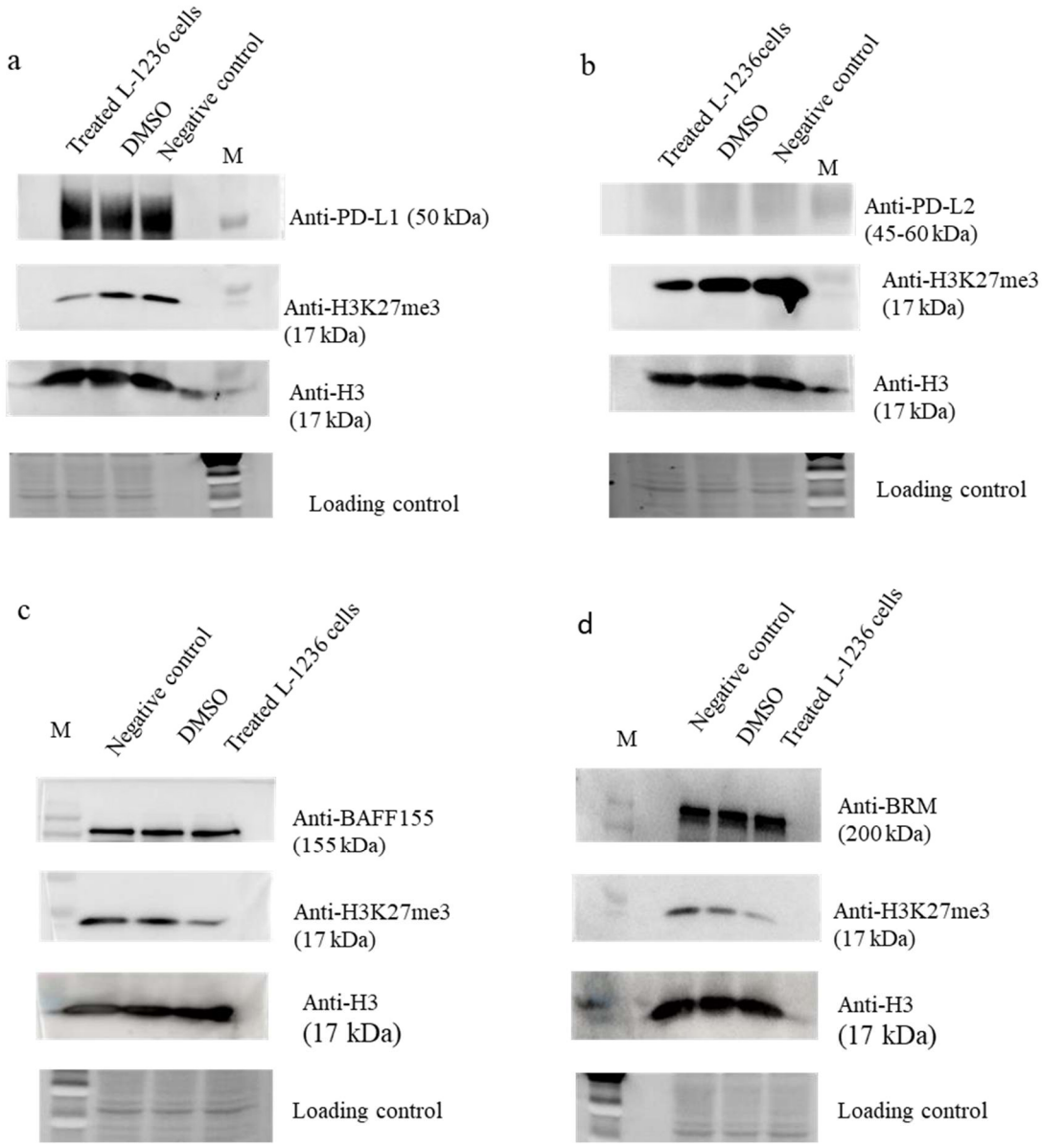

Figure 4.17: Effect of EPZ-6438 inhibitor on the expression pattern of targeted proteins.

The EPZ-6438 drug showed no significant impact on the expression of PD-L1, PD-L2, BAFF155 and BRM along with H3 histone the tri-methylated histone that showed a bit less abundance in treated cells of L-1236 cell line.

5. DISCUSSIONS

The first step in this study was to choose the cellular model of cHL with higher overexpression of PD-L1 protein. All HRS cell lines from repository of National Research Institute of Oncology : KM-H2, L-428 and L-1236 were used, in order to ensure that the cell lines are appropriate, authentication was performed by Eurofins, Germany, showing the proper genetic characteristics. Furthermore, the lines after defrosting were checked for the presence of characteristics that revealed that they are derived from HD patients. The examination of these lines revealed presence of HRS cells means: the presence of cells with two or more nuclei, the expression of diagnostic marker CD30 and PD-L1 expression (Küppers R & Hansmann, 2005). The confocal microscopy analysis exhibited the presence of bi- and multinucleated cells in mentioned cell lines (Gopas et al., 2016). The western blot analysis showed, that all cell line models exhibit the PD-L1 expression (with the L-1236 line representing the highest level of expression of PD-L1), providing the confirmation of cHL, a lymphatic malignancy origin of cell lines.

PD-L1 being a co-inhibitory factor diminishes immune responses to tumor cells and is responsible for tumorigenesis and progression subsequently. Thus overexpression of PD-L1 is reported in different types of cancers like: lung cancer, colorectal cancer, gastric cancer, bladder cancer, prostate cancer, and diffuse large B cell lymphoma (Han, Liu, & Li, 2020), that is line up to the overexpression of PD-L1 in our study in L-1236 Hodgkin lymphoma cell line. Overexpressed PDL1 promotes the immunosuppressive environment, as well as provides support for the migration and development to malignant cells simultaneously rather than sustaining depleted T-cell infiltration (Yu et al., 2020). PD-L1 function in cHL is considered altering the immunological environment, that's why, protects the tumor growth and survival (Carey et al., 2017).

Among different important ways of recognizing and confirming the HRS cells is the expression of the CD30 marker (120-KDa, type I trans membrane glycoprotein) from tumor necrosis factor superfamily. It functions as a marker mostly used for HRS diagnosis and may serve for verification of cHL cell lines. Thus, we check the presence of CD30 in all three cell lines (L-428, L-1236 and KM-H2). The expression of CD30 was found in all tested cell lines, what confirmed that they were cHL lymphoma cell lines indeed. This is consistent with findings that CD30 was also reported in previous studies on HRS cells (Sasse et al., 2019, Dumitru et al., 2023).

The molecular mechanism at the chromatin level that leads to overexpression from the PD-L1 promoter is not only a key to understanding the molecular based regulation of PD-L1, but also can be a clue for establishing a new therapy. SWI/SNF subunits like BRG1 and BRM ATPases and a Polycomb Repressive Complex 2 (PRC2) subunit – EZH2 participate in control of PD-L1 at chromatin level (Jancewicz et al., 2021) during CD4+ T cell exhaustion. Thus, keeping this in context, we tested the expression of SWI/SNF subunits BRM and INI1, and PRC2 subunit – EZH2 for all three cell line models (L-428, L-1236 and KM-H2). The most interesting fact has been observed in L-1236 cHL line, depicting the highest PD-L1 expression and showing the low expression of SWI/SNF subunits BRM and INI1 in contrast to high expression of EZH2, a PRC2 subunit. On the other side, KM-H2 cell line depicted low level of expression of PD-L1 and higher expression of BRM than for INI and EZH2. L-428 cell line also exhibits lower expression of PDL1, INI 1 and BRM but a bit higher of EZH2. This interplay of EZH2 and PD-L1 suggests, that this PRC2 complex may regulate the PD-L1 expression as described by a research study conducted in hepatoma cells, where the PD-L1 expression is induced by IFNγ due to down regulation of EZH2 (Xiao et al., 2019, or like in Jancewicz et al. where it was shown that EZH2 abundance on

PD-L1 promoter enhance, together with SWI/SNF BRG1 complex subunit, the PD-L1 expression. This observation makes the L-1236 cell line, with the significant overexpression of PD-L1 shown, an interesting object to be used for further experiments. Moreover, in L-1236 cell line the amplification of *CD274* (PD-L1) loci was observed (Green et al., 2010), what may be another level for PD-L1 expression regulation.

To confirm the observed relationships between the expression of examined proteins i.e. PD-L1, BRM and EZH2 at the transcript level, qRT-PCR was performed. The obtained data revealed again the highest expression of PD-L1 in L-1236 cell line, that well corresponds to PD-L1 abundance at the protein level. But surprisingly, on the transcript level the expression of *EZH2* gene and SWI/SNF subunits differ from that at protein level, and it provides a clue that the subunits might be regulated at protein level or mRNA stability level. There are different regulatory mechanisms that have been investigated involved in the upregulation of PD-L1 expression (Cha et al., 2019). In one study that included almost 41 samples from urothelial carcinoma and 59 samples from gastric cancer samples, the (*CD274*) mRNA expression levels

were measured by the qRT-PCR technique. In that study its quantity correlated to the immunotherapy response. The patients with more (*CD274*) mRNA expression responded better to the treatment (Kang et al., 2022).
Additionally, the mRNA level of *CD274* corresponds with PD-L1 protein abundance in those tested samples.

It has been previously demonstrated that PD-L1 is a trans-membrane protein and also localized into cellular nuclei (Cavazzoni et al., 2024). The PD-L1 basically interacts with endocytosis elements and nucleo-cytoplasmic transport pathways for its movement from the plasma membrane into the nucleus (Gao et al., 2020). The results of the nuclear PD-L1 fraction study show that PDL1 can translocate to the cell nucleus where it activates the transcription of some genes and modulates gene expression by direct interaction with chromatin-modifying complexes. The nuclear fraction basically sheds light on various complex molecular mechanisms in pathological conditions and makes it understandable. In addition to nuclear fraction the findings from FACS also revealed and confirmed that PD-L1 translocated not only to the nucleus but also was present on the cell surfaces (reported by Chan et al., 2022). The results from flow cytometry ensured the presence of PD-L1 (70.4%), PD-L2 (59.4%) and absence of PD-1 on the surface of L-1236 HRS cells. Additionally, the results once again confirmed sensitivity and specificity of this assay for cHL diagnosis (Roshal, Wood, & Fromm, 2011).

Chromatin immunoprecipitation (ChIP) on the *CD274* promoter region was performed on the selected HRS cell line (L-1236) followed by q-PCR, in order to explore if subunits of SWI/SNF and PCR2 complexes may bind and regulate the expression of *CD274* - PD-L1 encoding gene. The chromatin immunoprecipitation assay using antibodies of SWI/SNF and PRC2 subunits at *CD274* promoter was conducted according to (Jancewicz et al., 2021) for T-cells. In this study, the obtained results revealed that SWI/SNF subunit BAF155, PCR2 subunit EZH2, methylated histone, acetylated histone and PD-L1 were located on the same positions (-606, -495 and -259) at *CD274* locus. These results provide us the information about the involvement of SWI/SNF and PRC2 subunits and PD-L1 itself in the regulation of CD274 expression in HRS cells. Previous studies revealed that there was a functional antagonism between SWI/SNF subunits and EZH (PRC2) that plays crucial role in the regulation of gene expression (Kalimuthu & Chetty, 2016), but in some cases for particular gene the SWI/SNF complex acts synergistically with PRC2

complex regulating their expression (Sarnowska et al. 2016). A similar phenomenon of regulation has been proposed to be applied to the regulation of PD-L1 expression at transcriptional level in HRS cell, where SWI/SNF main subunit BAF155 binds in the same region with EZH2 subunit of PRC2 complex. This can suggest synergy between those two complexes in PD-L1 regulation of expression. . However, the relevance of this relationship in context of gene regulation in other types of cancer still needs more research in order to completely understand the mechanism. The presence of Histone marks (H3K27me3 and H3K27Ac) at the PD-L1 locus suggests the modulation of the PD-L1 expression either by activating or inhibiting transcription dynamically. Surprisingly, nuclear PD-L1 was present together with SWI/SNF subunits (BAF155), and EZH2 - a subunit of PRC2 complex on CD274 promoter region what indicates a collaborative regulatory mechanism, pointing to a positive feedback loop where PD-L1 may regulate its own expression in HRS cells. Together with SWI/SNF, PRC2 and PD-L1 the methylated and acetylated H3 on K27 was found in the same positions. Our findings are in consistence with another previously described study (Mittal & Roberts, 2020), where SWI/SNF complexes commonly cluster at the same position to histone H3 lysine 27 acetylation (H3K27ac) and promote active transcription by working with transcription factors by facilitating an open chromatin state. The EZH2 at the same location may work oppositely or synergistically by putting H3K27 trimethylation (H3K27me3) as a suppressive mark inhibiting gene expression. This is similar to the mechanism described by (Kim et al., 2018) where they studied the involvement of EZH2 in the activation of androgen receptor (AR) without dependency on the PRC2-Polycomb and methylation-independent roles of EZH2 as a transcription activator. Another research analysis revealed similar phenomena, when H3K27me3 ispresent, it causes disruption in normal histone modification thus leading to accumulation of H3K27ac. This rise in acetylated histone implies activation of chromatin state and is responsible for transcription and expression of the particular gene (Kim& Roberts, 2016). The findings from ChIP assay agree with such investigation. In another investigation, the regulation of PD-L1 transcription by the NFκB in human ovarian cancer cells was reported by ChIP assay. The overexpression of PD-L1 was analyzed by binding of acetylated p65 to the PD-L1 promoter region (Zou, Padmanabhan &Vancurova, 2020). In addition to this, an unbalanced epigenetic antagonistic interaction between the SWI/SNF subunits and the EZH2 (PRC2) resulted in INI1 depletion and thus promoted tumorgenesis. But on the other side, inhibiting EZH2 exhibits

profound therapeutic effect. An inclusive investigation of genome-wide chromatin and transcriptome profiles revealed substantial EZH2 occupancy not only at H3K27me3-marked genomic loci but also at promoters unrelated to PRC2, supporting EZH2 non-canonical involvement in ovarian cancer (Xiao et al., 2019).

My results of the chromatin immunoprecipitation (ChIP) on PD-L1 loci show the presence of both methylation and acetylation of histone H3K27 at the same positions of the *CD 274* promoter (606,-499,-259, +107). Both modifications are not possible at the same time at a given lysine of the histone H3 molecule. Moreover, they usually have the opposite epigenetic effect at the chromatin level. One possible explanation is the described amplification of the *PD-L1* and *PD-L2* genes in the chromosomal 9p24.1 region in various cell lines of Hodgkin lymphoma, including the L-1236 used in my experiments (Green et al., 2010). There is a possibility that different gene copies could undergo different epigenetic regulation. Exactly the same explanation could come from the wellknown fact, one of the cHL hallmark features - the common presence of bi- and multinucleated HRS cells (the result also shown above in the results of this thesis). It cannot be ruled out that even entire nuclei could undergo different epigenetic regulation. Another assumption is that even the same region of chromatin might be in a state where it is neither fully expressed nor fully repressed, being in a kind of equilibrium. It could be switched to fully active or repressed in the response to some cell signals.

For detailed understanding of nuclear PD-L1 function it is also important to know its nuclear partners and interactors. The co-immunoprecipitation from nuclear fraction using anti-PD-L1 antibody reveled that PD-L1 my interact in the nucleus with EZH2, BAF155 and INI1, a subunits of PRC2 and SWI/SNF complexes, what is in line with previous findings, that both those complexes together with PD-L1 bind to the promoter region of CD274 loci. Based on mass spectrometry results obtained after co-immunoprecipitation of PD-L1 it has been found that PDL1 may interact in the nucleus with the splicing machinery, thus regulating the RNA splicing and influencing the alternative choice of splice sites (Table 4.1). FUS RNA-binding protein, one of the found nuclear partners of PD-L1 was suggested to be involved in maintaining genomic stability as well as regulation of gene expression. It was selected for further confirming its interaction with isoforms I and IV of PD-L1 protein. Other candidate proteins chosen for this experimental line were BAFF155, AMPK, SLUG and SNAIL. The analysis was performed by

yeast two-hybrid system (Y2H). It has been confirmed that with the exception of AMPK, the above-mentioned proteins are the nuclear partners or protein interactors of PD-L1 protein. The interaction between the components of SWI/SNIF chromatin remodeling complex and PD-L1 is assumed to be involved in up-regulation of PD-L1 expression and that highly expressed PD-L1 further cause suppression of anti-tumor immune responses.

Slug (SNAI2) and Snail (SNAI1) are key transcription factors which drive Epithelial to Mensenchymal Transition (EMT). They play different important roles during the development of organs and healing of wounds. They also facilitate tumor metastasis. Previous study related to breast cancer revealed that Slug promotes the expression of genes involved in cancer progression, like PLD2 (Phospholipase D2) while Snail suppresses it (Ganesan, Mallets, & GomezCambronero, 2016). Another research explored that EGF-induced EMT increases PD-L1 expression in salivary gland cancer, causing immunosuppression. EGF-induced PD-L1 expression is reduced if EGFR kinase activity is blocked by inhibitors such as erlotinib or AG1478, suggesting that active EGFR is necessary for PD-L1 expression (Wang et al., 2018). The result is line up with our study, where the correlation was found between epithelial-to-mesenchymal transition (EMT) markers (Snail, Slug) and PD-L1 expression, suggesting that they might be involved in regulation of PD-L1 expression in Hodgkin lymphoma cell line. Furthermore, there is robust relationship, we observed between PD-L1 overexpression and BAF155 a subunit of SWI/SNIF complex which is consistent with the results showed by (Jancewicz et al., 2021).

In order to check the effect of EPZ-6438 (tazemetostat), an epigenetic drug that inhibits EZH2, a key component of the Polycomb Repressive Complex 2 (PRC2), an MTT assay was performed, revealing some surprising results. Basically, EZH2 is responsible for catalyzing of methyl group addition to histone proteins, particularly histone H3 lysine 27 (H3K27). As the result, it causes gene repression through chromatin condensation. If the drug worked, it would stop the expression of the targeted gene. The results after western blotting of treated cells from L-1236 cell line treated with this inhibitor revealed the dynamic expression of PD-L1, PD-L2, BRM and BAFF155 proteins along with methylated histone and histone proteins. It suggests that the inhibitor does not stop the expression of described proteins. The inhibitor EPZ-6438 prevents the methylation of H3K27 by blocking EZH2 but did not reduce the cell viability and PD-L1 expression. Although reduce the H# trimethylation on K27 position. The obtained results may

suggest that EZH2 inhibitor may work on PD-L1 loci after longer exposition or that PD-L1 gene is very precisely regulated due to their crucial function to suppress the immune response. There may be other alternative pathways or mechanisms involved in PD-L1 regulation or maybe EZH2 is not very crucial for PD-L1 modulation. Other factors that are essential for regulation of PD-L1 still need to be explored. Combination therapies targeting multiple pathways or exploiting vulnerabilities in resistant cancer cells hold promise for addressing the novel strategy to combat cHL.

6. CONCLUSION

The observation of PD-L1 overexpression in the studied L-1236 cell line originating from classical

Hodgkin lymphoma is considered the best model for studying the molecular mechanisms of PDL1 overexpression. The current study provides valuable information about its regulation at the transcript and protein levels, including its potential nuclear partners and their functions. Moreover, it provides a platform for in-depth analysis of its association with and regulation by SWI/SNF complex and EZH2- a critical subunit of the Polycomb Repressive Complex 2 (PRC2).

The work presented in this thesis focuses on the relatively new and not yet well known functions of PD-L1 fraction translocating to the cell nucleus. Results presented here undoubtedly prove the significance of this mechanism and suggest its engagement in the regulation of crucially important molecular mechanisms like posttranscriptional RNA processing and epigenetic modifications of the chromatin conducted with the cooperation of SWI/SNF and PRC2 complexes.

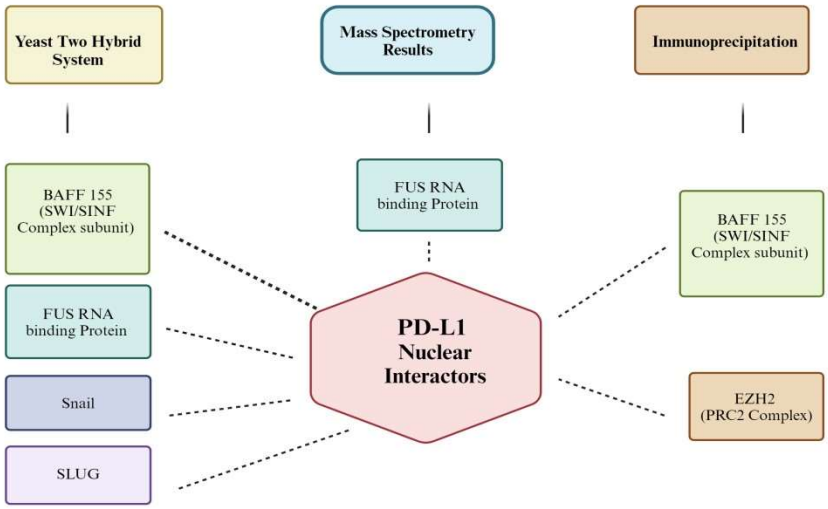

Figure 6.1: Interactome analysis of potential nuclear PD-L1 interactors.

Protein-protein interactions after immunoprecipitation, mass spectrometry analysis and particular confirmatory assays, including Yeast two-hybrid system, shed light on the complex network of

molecular interactions of PD-L1 within Hodgkin cells (Figure 6.1). The interaction of PD-L1 with its potential interactors offers valuable insight into their function in signaling pathways at the transcript level as determined by chromatin immunoprecipitation and at the protein level as determined by western blot analysis and Yeast two-hybrid assay. PD-L1 interaction with EZH2, BAFF155, FUS, SNAIL, and SLUG implies their involvement in regulating PD-L1 expression along with other cellular functions in the nucleus. This interaction may impact mRNA stability, processing, and splicing. One interesting fact can be the failure of modern therapies, that antiPDL1 cannot be transported to nucleus of HRS cell thus causing the growth and proliferation of tumour cell (Figure 6.2). The interplay could offer new therapeutic targets and strategies for manipulating PD-L1 expression. Additionally, the nuclear PD-L1 can serve as a new potential target for relapse cHL treatment.

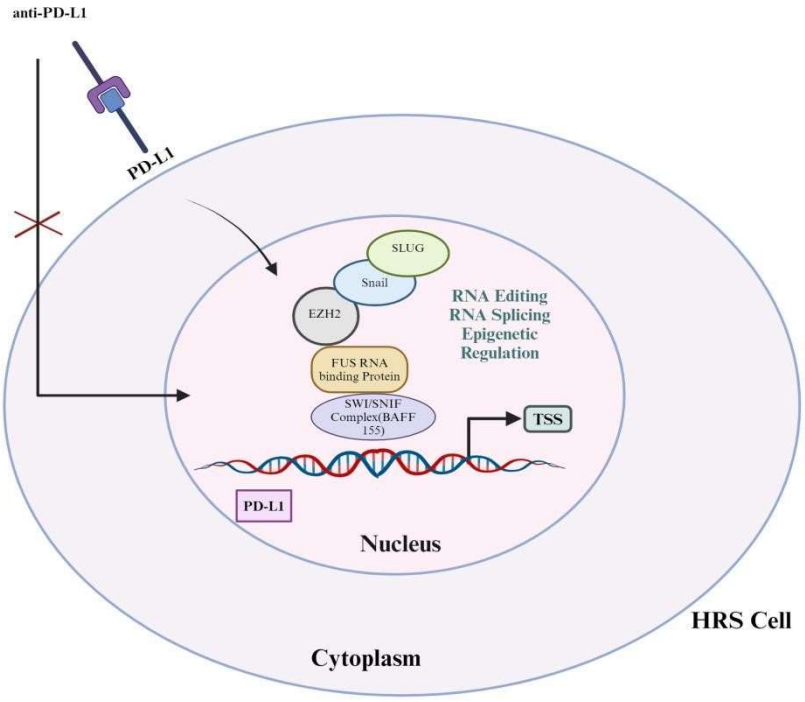

Figure 6.2: A systematic mechanism of PD-L1 inside the nucleus and cell surface of cHL.

The relationship between EZH2-mediated H3K27 methylation and PD-L1 expression is contextdependent and complicated. EZH2 inhibition by EPZ drugs does not impact the expression of PDL1 in the model described herein. It suggests that several factors participate in

PD-L1 expression regulation in addition to EZH2. This may include the complexity of the tumour immunesuppressive microenvironment, tumour cell heterogeneity, alternative regulatory mechanisms, or compensatory pathways. So, that is why it needs not a single drug treatment but combination therapies that would target multiple pathways, resulting in better outcomes for patients.

7. REFERENCES

- Aldinucci, D., Gloghini, A., Pinto, A., De Filippi, R., & Carbone, A. (2010). The classical Hodgkin's lymphoma microenvironment and its role in promoting tumour growth and immune escape. The Journal of Pathology: A Journal of the Pathological Society of Great Britain and Ireland, 221(3), 248-263
- Alver, B. H., Kim, K. H., Lu, P., Wang, X., Manchester, H. E., Wang, W., ... & Roberts, C. W. (2017). The SWI/SNF chromatin remodelling complex is required for maintenance of lineage specific enhancers. Nature communications, 8(1), 14648.
- Bachmann, I. M., Halvorsen, O. J., Collett, K., Stefansson, I. M., Straume, O., Haukaas, S. A., ... &Akslen, L. A. (2006). EZH2 expression is associated with high proliferation rate and aggressive tumor subgroups in cutaneous melanoma and cancers of the endometrium, prostate, and breast. J Clin Oncol, 24(2), 268-273.
- Barbari, C., Fontaine, T., Parajuli, P., Lamichhane, N., Jakubski, S., Lamichhane, P., & Deshmukh, R. R. (2020). Immunotherapies and combination strategies for immunooncology. International journal of molecular sciences, 21(14), 5009.
- Bardhan, K., Anagnostou, T., &Boussiotis, V. A. (2016). The PD1: PD-L1/2 pathway from discovery to clinical implementation. Front Immunol. 2016; 7: 550.
- Blank, C., Gajewski, T. F., & Mackensen, A. (2005). Interaction of PD-L1 on tumor cells with PD-1 on tumor-specific T cells as a mechanism of immune evasion: implications for tumor immunotherapy. Cancer Immunology, Immunotherapy, 54, 307-314.
- Bray, F., Ferlay, J., Soerjomataram, I., Siegel, R. L., Torre, L. A., & Jemal, A. (2018). Global cancer statistics 2018: GLOBOCAN estimates of incidence and mortality worldwide for 36 cancers in 185 countries. CA: a cancer journal for clinicians, 68(6), 394424.
- Calabretta, E., & Carlo-Stella, C. (2020). The Many facets of CD38 in Lymphoma: from tumor–microenvironment cell interactions to acquired resistance to immunotherapy. Cells, 9(4), 802.
- Carey, C. D., Gusenleitner, D., Lipschitz, M., Roemer, M. G., Stack, E. C., Gjini, E., ... & Rodig, S. J. (2017). Topological analysis reveals a PD-L1-associated microenvironmental

- niche for Reed-Sternberg cells in Hodgkin lymphoma. Blood, The Journal of the American Society of Hematology, 130(22), 2420-2430.

  Cavazzoni, A., Digiacomo, G., Volta, F., Alfieri, R., Giovannetti, E., Gnetti, L., ... & Tiseo, M. (2024). PD-L1 overexpression induces STAT signaling and promotes the secretion of pro-angiogenic cytokines in non-small cell lung cancer (NSCLC). Lung Cancer, 187, 107438.
- Centore, R. C., Sandoval, G. J., Soares, L. M. M., Kadoch, C., & Chan, H. M. (2020). Mammalian SWI/SNF chromatin remodeling complexes: emerging mechanisms and therapeutic strategies. Trends in Genetics, 36(12), 936-950.
- Cha, J. H., Chan, L. C., Li, C. W., Hsu, J. L., & Hung, M. C. (2019). Mechanisms controlling PD-L1 expression in cancer. Molecular cell, 76(3), 359-370.
- Chan, A., Scarpa Carniello, J. V., Gao, Q., Sigler, A., Baik, J., Roshal, M., & Lin, O. (2022). Role of flow cytometric immunophenotyping for classic Hodgkin lymphoma in small biopsy and cytology specimens. Archives of pathology & laboratory medicine, 146(4), 462-468.
- Dinand, V., & Arya, L. S. (2006). Epidemiology of childhood Hodgkin's disease: is it different in developing countries. Indian pediatrics, 43(2), 141.
- Dong, H., Zhu, G., Tamada, K., & Chen, L. (1999). B7-H1, a third member of the B7 family, co-stimulates T-cell proliferation and interleukin-10 secretion. Nature medicine, 5(12), 1365-1369.
- Dong, Y., Sun, Q., & Zhang, X. (2017). PD-1 and its ligands are important immune checkpoints in cancer. Oncotarget, 8(2), 2171.
- Dumitru, A. V., Țăpoi, D. A., Halcu, G., Munteanu, O., Dumitrascu, D. I., Ceaușu, M. C., &Gheorghișan-Gălățeanu, A. A. (2023). The Polyvalent Role of CD30 for Cancer Diagnosis and Treatment. Cells, 12(13), 1783.
- Euskirchen, G., Auerbach, R. K., & Snyder, M. (2012). SWI/SNF chromatin-remodeling factors: multiscale analyses and diverse functions. Journal of Biological Chemistry, 287(37), 30897-30905.
- Freeman, G. J., Long, A. J., Iwai, Y., Bourque, K., Chernova, T., Nishimura, H., ... &

•
Honjo, T. (2000). Engagement of the PD-1 immunoinhibitory receptor by a novel B7 family member leads to negative regulation of lymphocyte activation. The Journal of experimental medicine, 192(7), 1027-1034.

- Gan, L., Yang, Y., Li, Q., Feng, Y., Liu, T., & Guo, W. (2018). Epigenetic regulation of cancer progression by EZH2: from biological insights to therapeutic potential. Biomarker research, 6(1), 1-10.
- Ganesan, R., Mallets, E., & Gomez-Cambronero, J. (2016). The transcription factors Slug (SNAI2) and Snail (SNAI1) regulate phospholipase D (PLD) promoter in opposite ways towards cancer cell invasion. Molecular oncology, 10(5), 663-676.
- Gao, Y., Nihira, N. T., Bu, X., Chu, C., Zhang, J., Kolodziejczyk, A., ... & Wei, W. (2020). Acetylation-dependent regulation of PD-L1 nuclear translocation dictates the efficacy of anti-PD-1 immunotherapy. Nature cell biology, 22(9), 1064-1075.
- Gopas, J., Stern, E., Zurgil, U., Ozer, J., Ben-Ari, A., Shubinsky, G., ... &Livneh, E. (2016).
  Reed-Sternberg cells in Hodgkin's lymphoma present features of cellular senescence. Cell Death & Disease, 7(11), e2457-e2457.
- Gounder, M. M., Zhu, G., Roshal, L., Lis, E., Daigle, S. R., Blakemore, S. J., ... & Hollmann, T. J. (2019). Immunologic correlates of the abscopal effect in a SMARCB1/INI1-negative poorly differentiated chordoma after EZH2 inhibition and radiotherapy. Clinical Cancer Research, 25(7), 2064-2071.
- Green, M. R., Monti, S., Rodig, S. J., Juszczynski, P., Currie, T., O'Donnell, E., ... & Shipp, M. A. (2010). Integrative analysis reveals selective 9p24. 1 amplification, increased PD-1 ligand expression, and further induction via JAK2 in nodular sclerosing Hodgkin lymphoma and primary mediastinal large B-cell lymphoma. Blood, The Journal of the American Society of Hematology, 116(17), 3268-3277.
- Grufferman, S. E. Y. M. O. U. R., & Delzell, E. L. I. Z. A. B. E. T. H. (1984). Epidemiology of Hodgkin's disease. Epidemiologic reviews, 6, 76-106.
- Han, Y., Liu, D., & Li, L. (2020). PD-1/PD-L1 pathway: current researches in cancer. American journal of cancer research, 10(3), 727.

-
- Hanna, G. J., Lizotte, P., Cavanaugh, M., Kuo, F. C., Shivdasani, P., Frieden, A., ... & Haddad, R. I. (2018). Frameshift events predict anti–PD-1/L1 response in head and neck cancer. JCI insight, 3(4).

  Harris G. Hodgkin lymphoma different stages and risk factors. Hematol Blood Disord. 2022;5(5):12

  Huang, J., Pang, W. S., Lok, V., Zhang, L., Lucero-Prisno III, D. E., Xu, W., ... & NCD Global Health Research Group, Association of Pacific Rim Universities (APRU). (2022). Incidence, mortality, risk factors, and trends for Hodgkin lymphoma: a global data analysis.

  Journal of hematology & oncology, 15(1), 57.
- Ishida, Y., Agata, Y., Shibahara, K., & Honjo, T. (1992). Induced expression of PD-1, a novel member of the immunoglobulin gene superfamily, upon programmed cell death. The EMBO journal, 11(11), 3887-3895.
- Jancewicz, I., Siedlecki, J. A., Sarnowski, T. J., & Sarnowska, E. (2019). BRM: the core ATPase subunit of SWI/SNF chromatin-remodelling complex—a tumour suppressor or tumour-promoting factor. Epigenetics & chromatin, 12(1), 68.
- Jiang, H., Cao, H. J., Ma, N., Bao, W. D., Wang, J. J., Chen, T. W., ... & Xie, D. (2020). Chromatin remodeling factor ARID2 suppresses hepatocellular carcinoma metastasis via DNMT1-Snail axis. Proceedings of the National Academy of Sciences, 117(9), 4770-4780.
- Jose, B. O., Koerner, P., Spanos Jr, W. J., Paris, K. J., Silverman, C. L., Yashar, C., & Carrascosa, L. B. (2005). Hodgkin's lymphoma in adults--clinical features. The Journal of the Kentucky Medical Association, 103(1), 15-17.
- Kalimuthu, S. N., & Chetty, R. (2016). Gene of the month: SMARCB1. Journal of Clinical Pathology.
- Kang, S. Y., Heo, Y. J., Kwon, G. Y., & Kim, K. M. (2022). Expression of CD274 mRNA measured by qRT-PCR correlates with PD-L1 immunohistochemistry in gastric and urothelial carcinoma. Frontiers in Oncology, 12, 856444.

-
- Karantanos, T., Christofides, A., Bardhan, K., Li, L., &Boussiotis, V. A. (2016). Regulation of T cell differentiation and function by EZH2. Frontiers in immunology, 7, 172.
- Karantanos, T., Christofides, A., Bardhan, K., Li, L., &Boussiotis, V. A. (2016). Regulation of T cell differentiation and function by EZH2. Frontiers in immunology, 7, 172.
- Kaseb, H., & Babiker, H. M. (2023). Hodgkin Lymphoma. In StatPearls. StatPearls Publishing.
- Kaufman, H. L., Atkins, M. B., Subedi, P., Wu, J., Chambers, J., Joseph Mattingly, T., ... & Selig, W. K. (2019). The promise of Immuno-oncology: implications for defining the value of cancer treatment. Journal for immunotherapy of cancer, 7, 1-11.
- Kim, J., Lee, Y., Lu, X., Song, B., Fong, K. W., Cao, Q., ... & Yu, J. (2018). Polycomband methylation-independent roles of EZH2 as a transcription activator. Cell reports, 25(10), 2808-2820.
- Kim, K. H., & Roberts, C. W. (2016). Targeting EZH2 in cancer. Nature medicine, 22(2), 128-134.
- Kleer, C. G., Cao, Q., Varambally, S., Shen, R., Ota, I., Tomlins, S. A., ... & Chinnaiyan, A. M. (2003). EZH2 is a marker of aggressive breast cancer and promotes neoplastic transformation of breast epithelial cells. Proceedings of the national academy of sciences, 100(20), 11606-11611.
- Küppers, R., & Hansmann, M. L. (2005). The Hodgkin and reed/Sternberg cell. The international journal of biochemistry & cell biology, 37(3), 511-517.
- Lees, C., Keane, C., Gandhi, M. K., & Gunawardana, J. (2019). Biology and therapy of primary mediastinal B-cell lymphoma: current status and future directions. British journal of haematology, 185(1), 25-41
- Lin, D. Y. W., Tanaka, Y., Iwasaki, M., Gittis, A. G., Su, H. P., Mikami, B., ... &Garboczi, D. N. (2008). The PD-1/PD-L1 complex resembles the antigen-binding Fv domains of antibodies and T cell receptors. Proceedings of the National Academy of Sciences, 105(8), 3011-3016.

-
- Liu, C. Q., Xu, J., Zhou, Z. G., Jin, L. L., Yu, X. J., Xiao, G., ... & Zheng, L. (2018). Expression patterns of programmed death ligand 1 correlate with different microenvironments and patient prognosis in hepatocellular carcinoma. British journal of cancer, 119(1), 80-88
- Liu, Y., Wu, L., Tong, R., Yang, F., Yin, L., Li, M., ... & Lu, Y. (2019). PD-1/PD-L1 inhibitors in cervical cancer. Frontiers in Pharmacology, 10, 65.
- Marin-Acevedo, J. A., Dholaria, B., Soyano, A. E., Knutson, K. L., Chumsri, S., & Lou, Y. (2018). Next generation of immune checkpoint therapy in cancer: new developments and challenges. Journal of hematology & oncology, 11, 1-20.

  Masliah-Planchon, J., Bieche, I., Guinebretiere, J. M., Bourdeaut, F., & Delattre, O. (2015). SWI/SNF chromatin remodeling and human malignancies. Annual Review of Pathology:

  Mechanisms of Disease, 10, 145-171.
- Matsukawa, Y., Semba, S., Kato, H., Ito, A., Yanagihara, K., &Yokozaki, H. (2006). Expression of the enhancer of zeste homolog 2 is correlated with poor prognosis in human gastric cancer. Cancer science, 97(6), 484-491.
- Mauch, P. M., Kalish, L. A., Kadin, M., Coleman, C. N., Osteen, R., & Hellman, S. (1993). Patterns of presentation of Hodgkin disease. Implications for etiology and pathogenesis.

  Cancer, 71(6), 2062-2071.
- Medeiros, L. J., & Greiner, T. C. (1995). Hodgkin's disease. Cancer, 75(S1), 357-369.
- Meti, N., Esfahani, K., & Johnson, N. A. (2018). The role of immune checkpoint inhibitors in classical Hodgkin lymphoma. Cancers, 10(6), 204.
- Mittal, P., & Roberts, C. W. (2020). The SWI/SNF complex in cancer—biology, biomarkers and therapy. Nature reviews Clinical oncology, 17(7), 435-448.
- Morin, R. D., Johnson, N. A., Severson, T. M., Mungall, A. J., An, J., Goya, R., ... & Marra, M. A. (2010). Somatic mutations altering EZH2 (Tyr641) in follicular and diffuse large Bcell lymphomas of germinal-center origin. Nature genetics, 42(2), 181-185.

-
- Nishimura, H., Agata, Y., Kawasaki, A., Sato, M., Imamura, S., Minato, N., ... & Honjo, T. (1996). Developmentally regulated expression of the PD-1 protein on the surface of double-negative (CD4–CD8–) thymocytes. International immunology, 8(5), 773-780.
- Nomi, T., Sho, M., Akahori, T., Hamada, K., Kubo, A., Kanehiro, H., ... & Nakajima, Y. (2007). Clinical significance and therapeutic potential of the programmed death-1 ligand/programmed death-1 pathway in human pancreatic cancer. Clinical cancer research, 13(7), 2151-2157.
- Pileri, S. A., Ascani, S., Leoncini, L., Sabattini, E., Zinzani, P. L., Piccaluga, P. P., ... & Stein, H. (2002). Hodgkin's lymphoma: the pathologist's viewpoint. Journal of clinical pathology, 55(3), 162-176.
- Radkiewicz, C., Bruchfeld, J. B., Weibull, C. E., Jeppesen, M. L., Frederiksen, H., Lambe, M., ... & Wästerlid, T. (2023). Sex differences in lymphoma incidence and mortality by subtype: A population-based study. American Journal of Hematology, 98(1), 23-30.

  Ramos, P., Karnezis, A. N., Craig, D. W., Sekulic, A., Russell, M. L., Hendricks, W. P., ... & Trent, J. M. (2014). Small cell carcinoma of the ovary, hypercalcemic type, displays frequent inactivating germline and somatic mutations in SMARCA4. Nature genetics, 46(5), 427-429.
- Rao, X., Huang, X., Zhou, Z., & Lin, X. (2013). An improvement of the 2ˆ (–delta delta CT) method for quantitative real-time polymerase chain reaction data analysis. Biostatistics, bioinformatics and biomathematics, 3(3), 71.
- Reisman, D. N., Sciarrotta, J., Wang, W., Funkhouser, W. K., & Weissman, B. E. (2003). Loss of BRG1/BRM in human lung cancer cell lines and primary lung cancers: correlation with poor prognosis. Cancer research, 63(3), 560-566.
- Ribatti, D., Tamma, R., Annese, T., Ingravallo, G., &Specchia, G. (2022). Inflammatory microenvironment in classical Hodgkin’s lymphoma with special stress on mast cells. Frontiers in Oncology, 12.

-
- Roshal, M., Wood, B. L., & Fromm, J. R. (2011). Flow cytometric detection of the classical Hodgkin lymphoma: clinical and research applications. Advances in hematology, 2011.
- Salmaninejad, A., Khoramshahi, V., Azani, A., Soltaninejad, E., Aslani, S., Zamani, M. R., ... & Hosseini, S. M. (2018). PD-1 and cancer: molecular mechanisms and polymorphisms. Immunogenetics, 70, 73-86.
- Sarnowska, E., Gratkowska, D. M., Sacharowski, S. P., Cwiek, P., Tohge, T., Fernie, A. R., ... & Sarnowski, T. J. (2016). The role of SWI/SNF chromatin remodeling complexes in hormone crosstalk. Trends in plant science, 21(7), 594-608.
- Sarnowska, E., Gratkowska, D. M., Sacharowski, S. P., Cwiek, P., Tohge, T., Fernie, A. R., ... & Sarnowski, T. J. (2016). The role of SWI/SNF chromatin remodeling complexes in hormone crosstalk. Trends in plant science, 21(7), 594-608.
- Sasse, S., Reddemann, K., Diepstra, A., Oschlies, I., Schnitter, A., Borchmann, S., ... & Klapper, W. (2019). Programmed cell death protein-1 (PD-1)-expression in the microenvironment of classical Hodgkin lymphoma at relapse during anti-PD-1-treatment. Haematologica, 104(1), e21.
- Savas, S., &Skardasi, G. (2018). The SWI/SNF complex subunit genes: Their functions, variations, and links to risk and survival outcomes in human cancers. Critical reviews in oncology/hematology, 123, 114-131.

  Smith, C. M., & Friedman, D. L. (2022). Advances in Hodgkin lymphoma: including the patient's voice. Frontiers in Oncology, 12, 855725.
- Sun, C., Mezzadra, R., & Schumacher, T. N. (2018). Regulation and function of the PDL1 checkpoint. Immunity, 48(3), 434-452
- Takeshima, H., Niwa, T., Takahashi, T., Wakabayashi, M., Yamashita, S., Ando, T., ... & Ushijima, T. (2015). Frequent involvement of chromatin remodeler alterations in gastric field cancerization. Cancer letters, 357(1), 328-338.
- Tang, L., Nogales, E., & Ciferri, C. (2010). Structure and function of SWI/SNF chromatin remodeling complexes and mechanistic implications for transcription. Progress in biophysics and molecular biology, 102(2-3), 122-128.

-
- Thomas, R. K., Re, D., Wolf, J., & Diehl, V. (2004). Part I: Hodgkin's lymphoma—molecular biology of Hodgkin and Reed-Sternberg cells. The lancet oncology, 5(1), 11-18.
- Tolstorukov, M. Y., Sansam, C. G., Lu, P., Koellhoffer, E. C., Helming, K. C., Alver, B. H., ... & Roberts, C. W. (2013). Swi/Snf chromatin remodeling/tumor suppressor complex establishes nucleosome occupancy at target promoters. Proceedings of the National Academy of Sciences, 110(25), 10165-10170.
- Topalian, S. L., Drake, C. G., &Pardoll, D. M. (2015). Immune checkpoint blockade: a common denominator approach to cancer therapy. Cancer cell, 27(4), 450-461.
- Townsend, W., &Linch, D. (2012). Hodgkin's lymphoma in adults. The Lancet, 380(9844), 836-847.
- Townsend, W., &Linch, D. (2012). Hodgkin's lymphoma in adults. The Lancet, 380(9844), 836-847.
- Valencia, A. M., Collings, C. K., Dao, H. T., Pierre, R. S., Cheng, Y. C., Huang, J., ... &Kadoch, C. (2019). Intellectual disability-associated SMARCB1 mutations reveal a nucleosome acidic patch interaction site that potentiates mSWI/SNF chromatin remodeling. Cell, 179(6), 1342.
- Versteege, I., Sévenet, N., Lange, J., Rousseau-Merck, M. F., Ambros, P., Handgretinger, R., ... & Delattre, O. (1998). Truncating mutations of hSNF5/INI1 in aggressive paediatric cancer. Nature, 394(6689), 203-206.
- Wang, H. W., Balakrishna, J. P., Pittaluga, S., & Jaffe, E. S. (2019). Diagnosis of Hodgkin lymphoma in the modern era. Br J Haematol, 184(1), 45-59.

  Wang, H. W., Balakrishna, J. P., Pittaluga, S., & Jaffe, E. S. (2019). Diagnosis of Hodgkin lymphoma in the modern era. British journal of haematology, 184(1), 45-59.
- Wang, J., Seebacher, N., Shi, H., Kan, Q., & Duan, Z. (2017). Novel strategies to prevent the development of multidrug resistance (MDR) in cancer. Oncotarget, 8(48), 84559.
- Wang, Y., Hu, J., Wang, Y. A., Ye, W., Zhang, X., Ju, H., ... & Liu, S. (2018). EGFR activation induced Snail-dependent EMT and myc-dependent PD-L1 in human salivary adenoid cystic carcinoma cells. Cell cycle, 17(12), 1457-1470.

-
- Wei, S. C., Duffy, C. R., & Allison, J. P. (2018). Fundamental mechanisms of immune checkpoint blockade therapy. Cancer discovery, 8(9), 1069-1086.
- Weikert, S., Christoph, F., Köllermann, J., Müller, M., Schrader, M., Miller, K., & Krause, H. (2005). Expression levels of the EZH2 polycomb transcriptional repressor correlate with aggressiveness and invasive potential of bladder carcinomas. International journal of molecular medicine, 16(2), 349-353
- Workman, J. L., & Kingston, R. E. (1998). Alteration of nucleosome structure as a mechanism of transcriptional regulation. Annual review of biochemistry, 67(1), 545-579.
- Xia, Q. Y., Rao, Q., Cheng, L., Shen, Q., Shi, S. S., Li, L., ... & Zhou, X. J. (2014). Loss of BRM expression is a frequently observed event in poorly differentiated clear cell renal cell carcinoma. Histopathology, 64(6), 847-862.
- Xiao, G., Jin, L. L., Liu, C. Q., Wang, Y. C., Meng, Y. M., Zhou, Z. G., ... & Zheng, L. (2019). EZH2 negatively regulates PD-L1 expression in hepatocellular carcinoma. Journal for immunotherapy of cancer, 7(1), 1-15.
- Yamagishi, M., &Uchimaru, K. (2017). Targeting EZH2 in cancer therapy. Current opinion in oncology, 29(5), 375-381.
- Yamagishi, M., &Uchimaru, K. (2017). Targeting EZH2 in cancer therapy. Current opinion in oncology, 29(5), 375-381.
- Yamagishi, M., &Uchimaru, K. (2017). Targeting EZH2 in cancer therapy. Current opinion in oncology, 29(5), 375-381.
- Yu, W., Hua, Y., Qiu, H., Hao, J., Zou, K., Li, Z., ... & Deng, W. (2020). PD-L1 promotes tumor growth and progression by activating WIP and β-catenin signaling pathways and predicts poor prognosis in lung cancer. Cell death & disease, 11(7), 506.

  Zhou, M., Yuan, J., Deng, Y., Fan, X., & Shen, J. (2021). Emerging role of SWI/SNF complex deficiency as a target of immune checkpoint blockade in human cancers. Oncogenesis, 10(1), 3.
- Zou, Y., Padmanabhan, S., &Vancurova, I. (2020). Analysis of PD-L1 transcriptional regulation in ovarian cancer cells by chromatin immunoprecipitation. Immune Mediators in Cancer: Methods and Protocols, 229-239.

LIST OF FIGURES

LIST OF TABLES